

# Hydro-plastic response of beams and stiffened panels subjected to extreme water slamming at small impact angles, Part I: An analytical solution

Zhaolong Yu <sup>a, b\*</sup>, Jørgen Amdahl <sup>a, b</sup>, Marilena Greco <sup>a, b, c</sup>, Huili Xu <sup>a, b</sup>

a, Centre for Autonomous Marine Operations and Systems (AMOS), Norwegian University of Science and Technology (NTNU), Norway

b, Department of Marine Technology, Norwegian University of Science and Technology (NTNU), Norway

c. CNR-INM, Institute of Marine Engineering, Rome, Italy

## Abstract

Water impact (slamming) is a strongly nonlinear phenomenon including significant fluid structure interactions. In the case of slamming with a small impact angle between the structure and water, the coupling between hydrodynamic pressure and the elastic responses of structures, known as hydroelasticity, matters. This has been studied extensively. However, when structures are subjected to violent water slamming in extreme sea states, large stresses may occur that exceed the material yield stress, causing large plastic flow and permanent damage. In such cases, the plastic responses of a structure will be strongly coupled with the hydrodynamic pressure, termed as hydro-plasticity. Hydro-plastic slamming has rarely been studied before.

This is Part I of a two-part companion paper. The paper advances the state-of-the-art of hydro-plastic slamming by formulating, for the first time, an analytical model coupling the hydrodynamic forces and the plastic response of rectangular beams and one-way stiffened panels. The studied scenarios are flat or nearly flat water impacts, which are critical for hydro-plasticity excitation. The impact angle between the water free surface and the structure should preferably be no larger than  $5^\circ$ . Based on the proposed model, the governing non-dimensional parameters for hydro-plastic slamming are identified and discussed. Design curves for plate strips and stiffened panels against extreme slamming are developed. Part II-*Numerical verification and analysis* presents numerical verification and discussion of the analytical model by comparing with results from the multi-material Arbitrary Lagrangian Eulerian (ALE) simulations.

The proposed analytical model does not require the challenging estimation of pressure history that is normally used in the design against slamming. Only the initial impact velocity is needed as the main input. The resulting non-dimensional curves may be utilized in rules and standards for the design of ships and offshore structures against extreme slamming loads.

**Key words:** water slamming; hydro-plasticity; analytical solution; beams and stiffened panels; travelling hinge; permanent deflection

## Nomenclature

$2L$	Length of the beam
$h$	Rectangular beam height/stiffener web height
$b$	Rectangular beam width/Distance between stiffeners
$x$	$x$ coordinate
$X$	Distance of the travelling hinge relative to the beam end
$A_t$	Area of the top flange of a stiffened panel cross section
$A_w$	Area of the web of a stiffened panel cross section
$A_s = A_w + A_t$	Area of the stiffener cross section including web and top flange
$A_p$	Area of the plate flange of a stiffened panel cross section
$A_e$	Area of the whole cross section
$w(x,t)$	Lateral deflection of the beam
$w_{mode}$	Structural deformation mode with unit central deflection
$v(x,t)$	Velocity field of the beam
$V_0$	Initial water-entry velocity of the beam
$V_m$	Nodal deflection velocity at the beam middle span
$t$	Time
$\delta$	Beam central deflection
$\delta_p$	Beam permanent central deflection
$\sigma_y$	Yield stress of the material
$\rho$	Density of water
$m$	Mass of the beam per unit length
$M_s$	Generalized structural mass
$M_a$	Generalized added mass of the beam
$K$	Generalized structural stiffness of the beam
$M_0$	Fully plastic bending moment of the beam
$M$	Bending moment of the beam
$N$	Membrane force of the beam
$N_0$	Fully plastic yield resistance in tension
$e$	Total elongation for half a beam
$\theta$	Total rotation angle at hinges considering half a beam
$\varphi$	Velocity potential due to the body motion assuming that the velocity equals the mode shape
$\phi$	Total velocity potential due to body motion connected with $\varphi$
$g$	Gravitational acceleration
$p$	Hydrodynamic pressure due to body motion
$p\varphi$	Hydrodynamic pressure connected with $\varphi$
$\omega$	Angular velocity of the beam segment
$\omega_{dry}$	Dry natural frequency of the first mode shape
$\omega_{wet}$	Wet natural frequency of the first mode shape
$(\dot{\quad})$	Time derivative

## 1. Introduction

Ships and offshore structures operating at sea are exposed to the risk of violent water impacts (slamming). Loads connected with blunt impacts, i.e. the angle between the body and the water is small, and with large relative body-water velocity, are highly impulsive and transient, characterized by high pressure peaks and small durations. Potential consequences of slamming impacts may vary from small structural vibrations to large permanent deformations and structural damage. In the extreme sea states, slamming loads may cause progressive collapse of structures and threaten human lives. An example is the collapse of a Japanese container ship after violent bow flare slamming impacts on a heavy sea state in the North Pacific Ocean in 1978 (Yamamoto et al., 1985). The inner structures, such as longitudinals, web frames and side stringers, collapsed, and the deck and shell plating buckled. More recently in 2015, a tragic slamming incident occurred on the offshore drilling rig *COSL Innovator* in the North Sea, where a steep horizontal wave struck the unit on the port side of the front bulkhead of the forward box girder. Water intrusion caused extensive damage to cabins. One person was killed and four were injured. After the incident, simple guidelines such as DNVGL-OTG-13 (2016) and DNVGL-OTG-14 (2016) were introduced for designing offshore structures against violent slamming loads.

Slamming may be defined as any water impact wherever it occurs if it satisfies the following condition: the impact duration is short (Bereznitski, 2001). Various scenarios may lead to slamming. For ships, bottom slamming may occur when large heave and pitch motions force a portion of the ship bottom to exit and re-enter the water (see plot (a) of Fig. 1). High speed vessels such as catamarans are likely to experience severe wetdeck slamming (see plot (b) of Fig. 1) (Faltinsen, 2005). Another scenario is green water on deck or extreme waves (see plot (c) of Fig. 1). Other ship slamming scenarios include sloshing induced slamming inside a partially-filled tank (see plot (d) of Fig. 1), free falling lifeboats, dropped objects, etc. Offshore structures often work at a specific location for a long time period, which increases their exposure to extreme waves (see plots (e) and (f) of Fig. 1). It is important that the design ensures a sufficiently large air gap, i.e. vertical distance between the underdeck and the sea surface, to avoid slamming, and sufficient structural strength of bottom plating in case slamming occurs.

Early studies on the slamming phenomenon can be dated back to the 1920s. von Karman (1929) and Wagner (1932) presented pioneering works, formulating analytical solutions to the pressure distribution and the time history in a rigid body water-entry problem. The von Karman and Wagner theories have been developed extensively by many researchers, such as Zhao and Faltinsen (1993) and Mei et al. (1999). Most wave-impact studies and design guidelines today have adopted the assumption that hydrodynamic loading is the same for rigid and deformable bodies. However, this is not always a valid assumption in practice. Bereznitski (2001) and Faltinsen (2005) showed that the structures could be considered as rigid if the ratio of the wetting time over structural natural period is large. When the ratio becomes small or comparable to the structural natural period, significant coupling between hydrodynamic pressure and the elastic structural responses, termed as hydroelasticity, will occur, and the rigid body assumption is no more valid. The hydroelastic response of structures under slamming were studied extensively by many researchers, such as Faltinsen (2000), Kvalsvold and Faltinsen (1995) and Bishop and Price (1979).

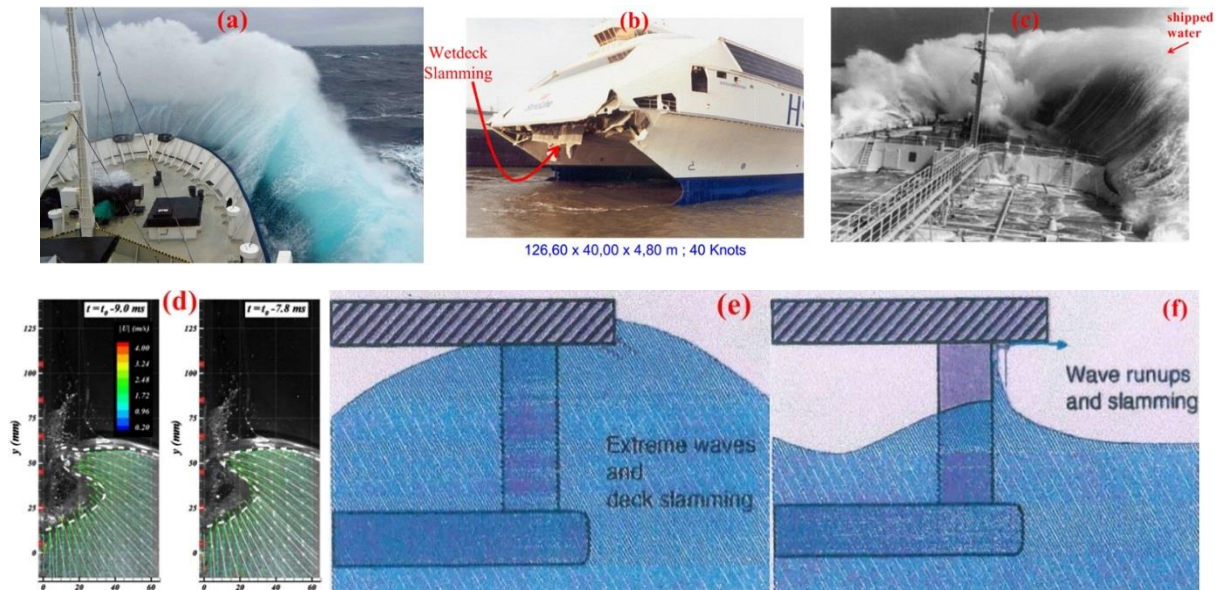


Fig. 1. Slamming in ships and offshore structures, (a) from Intelligent Engineering (2010), (b) from Amin et al. (2013), (c) photo by Per Meidel from Faltinsen (2005), (d) from Lugni et al. (2010), (e) and (f) from Baarholm (2001)

In practice, the structural response is not always in the elastic range. When violent slamming with a strong impulse occurs, the maximum stresses in the structures can exceed the material yield stress, causing large plastic flow and permanent deformations. In such cases, the strong interaction between hydrodynamic pressure and the elastoplastic response of structures is termed as ‘hydro-elastoplastic’. Hydro-elastoplastic slamming is a very complicated multi-disciplinary problem, and has not been studied much so far.

Theoretical studies for coupled hydro-elastoplastic or hydro-plastic slamming have not been reported in the literature. Because permanent deformations are of major concern when structural response enters the plastic range, the problem is often simplified by neglecting the coupling effect and assuming a certain shape of the temporal variation and distribution of the pressure. Taking the pressure history as input, theoretical solutions for blast loaded structures may be used for the slamming problem. Jones (1973) presented a simplified model for the permanent damage of fully clamped rectangular plates subjected to a pre-defined triangular slamming history. Jiang and Olson (1995) assumed a pressure history with exponential decay for underwater blast loading on stiffened panels. The structural responses of the panels were formulated with a travelling hinge solution assuming a rigid perfectly plastic material. Henke (1994) also assumed an exponentially decaying slamming pressure acting on the ship hull plating. The finite difference method was used to solve a plate strip formulation considering both elastic and elastic-plastic structural responses. More analytical solutions for the plastic responses of blast loaded beams, plates and shells can be found for instance in Symonds and Mentel (1958), Schubak et al. (1993a), Schubak et al. (1993c), Jones (2011), Symonds and Yu (1985). These models however do not include the coupling between fluid and structures.

The literature review shows that no coupled analytical solution exists for the hydro-elastoplastic slamming. This Part I of the two-part article aims at bridging the knowledge gap by presenting, in sections 2 to 5, a coupled analytical solution for the permanent deflections of beams and one-way

stiffened panels subjected to slamming. The studied scenarios are flat or nearly flat water impacts, where the impact angle between the water free surface and the structure should preferably be no larger than  $5^\circ$ . The elastic response of the structure is disregarded on the assumption that, in the extreme conditions, the elastic energy is small compared to the plastic strain energy. Based on the proposed model, in sections 6 and 7, governing non-dimensional parameters for the hydro-plastic slamming response of beams and stiffened panels are identified and discussed, and normalized design curves are recommended. Then main conclusions are drawn in section 8.

## 2. Modelling of plate strips and one-way stiffened panels subjected to slamming loads

Fully clamped one-way stiffened panels and beams with rectangular cross sections, i.e. plate strips with unit width, are considered. For one-way stiffened panels consisting of several bays (refer Fig. 2), a stiffener located some distance away from the lateral edges can be modeled as a beam where the associated plate constitutes a large flange.

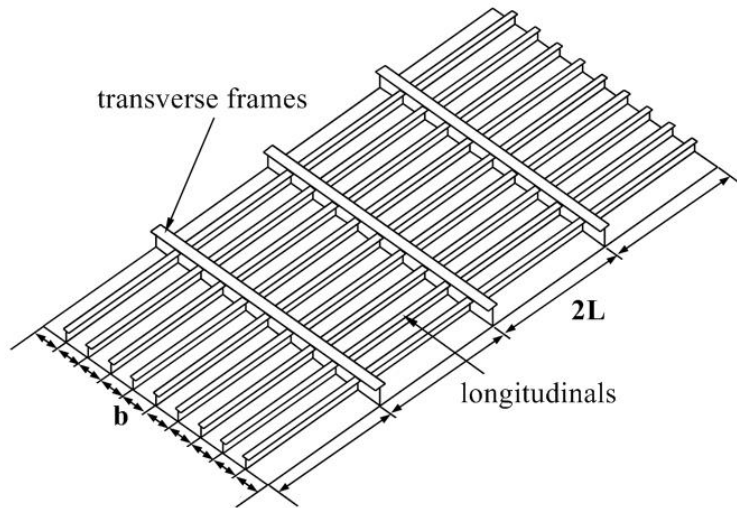


Fig. 2. A one-way stiffened panel

We follow Faltinsen (2005)'s assumption that, when *flat* beams (zero deadrise angle) are subjected to impulsive slamming loads, they will go through two phases, i.e. an initial structural inertial phase (also called the acoustic phase) and a later free-vibration phase. In the first phase, the structure experiences a large force impulse within a very short time relative to the highest structural natural period, i.e. the natural period of the slammed plates/stiffened panels. At the end of the first phase, the structure is imparted a deformation velocity averagely equal to the impact velocity  $V_0$ , while its deflection is virtually zero. As large plastic deformations occur in our second phase instead of only elastic vibrations considered by Faltinsen (2005), we name this phase as the free-deflection phase.

Given the initial conditions from the acoustic phase, the main focus is then to investigate the hydro-plastic coupling during the free-deflection phase. The hydrodynamic pressure experienced by the beam during this phase is discussed in *Section 3*. For the structural deformations, the following assumptions are introduced:

- (1). The elastic energy is small compared to the plastic strain energy, and can be disregarded.

(2). The material is rigid-perfectly plastic. This assumption is often adopted for collision analysis in accidental limit states, see the review paper by Yu and Amdahl (2018).

(3). The effects of strain rate and strain hardening can be neglected.

(4). The shear deformation is small and negligible. This assumption is considered to be reasonable when  $2L/h \geq 10$  according to Yu et al. (2018), where  $2L$  and  $h$  are the beam length and height, respectively.

(5). The deflections are finite, but still small compared to the beam length.

During the free-deflection phase, following the theory for blast loaded structures (Schubak et al., 1993b; Symonds and Mentel, 1958), beams subjected to water slamming are assumed to experience three different stages. They are labelled as stages 1 to 3 in Fig. 3 and correspond to the travelling hinge stage, the stationary hinge stage and the pure tension stage. Theoretically, the travelling hinge concept is introduced in order not to violate the generalized yield surface as explained in Jones (2011) when the loading pressure becomes very large. The deflections of the structure will induce fluid flow and cause hydrodynamic pressure distributed along the beam that interacts with the body deformations.

The deformation is symmetric about the beam vertical central axis, as observed experimentally e.g. by Shin et al. (2017), and we therefore consider only half of the beam. In the free deflection phase, the beam responds initially with a hinge travelling towards the middle, while the segment near the beam edge rotates as a rigid part about the support as shown in Fig. 3(a). The resulting beam deformation velocity, at time  $t$  from the start of the free-deflection phase, is:

$$v(x, X, t) = \begin{cases} \omega x & \text{if } 0 \leq x \leq X(t) \\ \omega X = V_m(t) & \text{if } X(t) < x \leq L \end{cases} \quad (1)$$

Here  $X$  is the distance of the travelling hinge from the support, and  $\omega$  is the angular velocity.  $V_m(t)$  is the nodal velocity, uniform in the beam middle span. This yields a linear acceleration field:

$$\dot{v}(x, X, t) = \begin{cases} \dot{\omega}(t)x & \text{if } 0 \leq x \leq X(t) \\ \dot{V}_m(t) & \text{if } X(t) < x \leq L \end{cases} \quad (2)$$

and a displacement field that is approximated to be linear:

$$w(x, X, t) \approx \begin{cases} \int_0^t V_m dt \cdot \frac{x}{X} & \text{if } 0 \leq x \leq X(t) \\ \int_0^t V_m dt & \text{if } X(t) < x \leq L \end{cases} \quad (3)$$

$$= \int_0^t V_m dt \cdot w_{\text{mode}}(X(t), x)$$

Here the super dot represents a time derivative, and  $w_{\text{mode}}(X(t), x) = \begin{cases} \frac{x}{X} & \text{if } 0 \leq x \leq X(t) \\ 1 & \text{if } X(t) < x \leq L \end{cases}$  is

the structural deformation mode in stage 1. The velocity field in Eq. (1) can be rewritten as  $v(x, X, t) = V_m(t) \cdot w_{\text{mode}}(X(t), x)$ .

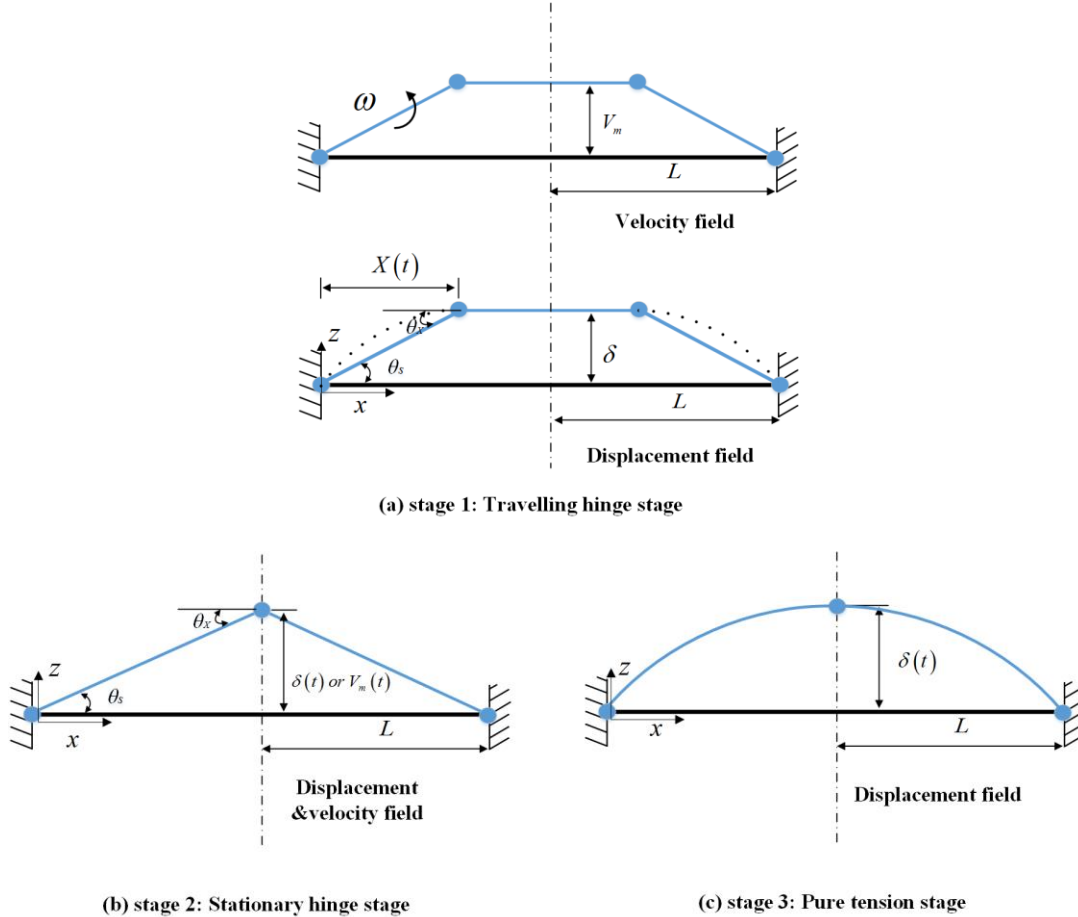


Fig. 3. Deformation stages of a beam during the free-deflection phase induced by slamming

In reality, a linear velocity field with a propagating hinge yields a curved displacement field. The exact shape of the displacement depends on the motion of the travelling hinge. Wierzbicki and Suh (1988) derived a solution to the indentation of tubes with freely propagating dent length, and the obtained displacement was parabolic. For the present problem, motions of the travelling hinge interact with beam deflections and the exact solution for the deflections is very complicated. Therefore, the displacement is assumed to be linear for simplicity.

Considering half of the fully clamped beam, the total elongation  $e$  and the elongation rate  $\dot{e}$  are

$$e = e_x + e_s = \sqrt{X^2 + \delta^2} - X \approx \frac{\delta^2}{2X}; \quad \dot{e} = \frac{\delta}{X} \dot{\delta} - \frac{1}{2} \left( \frac{\delta}{X} \right)^2 \dot{X} \quad (4)$$

where the subscripts  $X$  and  $S$  denote the variables estimated at the travelling hinge ( $x=X$ ) and at the support, respectively. Moreover,  $\delta$  is the deflection at the middle of the beam

The total rotation  $\theta$  and rotation rate  $\dot{\theta}$  at the hinges are:

$$\theta = \theta_x + \theta_s = \frac{2\delta}{X}; \quad \dot{\theta} = \frac{2\dot{\delta}}{X} - \frac{2\delta}{X^2} \dot{X} \quad (5)$$

The displacement  $\delta$  is a small value compared to  $X$ . By neglecting the second order terms in eqs. (4) and (5), we obtain,

$$\begin{aligned} \dot{\epsilon} &\approx \frac{\delta}{X} \dot{\delta}; \quad \dot{\theta} \approx \frac{2\dot{\delta}}{X} \\ \frac{\dot{\epsilon}}{\dot{\theta}} &= \frac{\delta}{2} \end{aligned} \quad (6)$$

When the travelling hinges from both beam ends meet in the beam middle span, stage 2 starts with a middle stationary hinge as shown in Fig. 3(b). As the deflection increases, the bending moment decreases while the membrane force increases. When the beam cross section becomes fully occupied by tensile yield stresses, the pure-tension stage 3 initiates. Permanent deflections are reached when the beam middle-span velocity  $V_m$  decreases to zero. Before studying structural deformations during these three stages, the hydrodynamic pressure acting on the beam needs to be modelled.

### 3. Hydrodynamic pressure acting on a beam during the free-deflection phase

As the impact angle approaches zero, the water-structure impact becomes flat and the pressure goes to infinity according to the incompressible-liquid models. This is unrealistic. The reason is that water compressibility will matter during an initial acoustic phase. With a flat structure, air cushion may be formed between the body and the water. Compressibility influences the flow of the air in the cushion and subsequently affects the water flow (Faltinsen, 2005). Kvals vold and Faltinsen (1995) carried out drop tests of aluminum and steel flat plates into a water tank, and found that the maximum pressure was very sensitive to small changes of the physical conditions. Drop tests were repeated with nearly the same water entry velocity, but the measured maximum pressure was very scattered as shown in Fig. 4. It is therefore not rational to focus on the peak pressures as structural design parameters.

On the basis of the model tests, Faltinsen (2005) simplified the water-entry problem of a flat plate as a structural-inertia phase and a free-vibration phase, here called the free-deflection phase to account for the large plastic deformations. In the structural inertia phase, a large impulse is imparted to the structure within a very short time relative to the structure highest natural period. As a consequence, the structure does not have enough time to build up deformations. Faltinsen (2005) stated that the details of the pressure distribution are not important in the structural inertia phase, but it is the impulse due to the impact that matters. As the impulse dies out, the second phase starts with the structure having a space-averaged deformation speed equal to the initial impact velocity



$V_0$ . In the present hydro-plastic slamming analysis, we assume that the free-deflection phase starts with the beam middle portion (between two travelling hinges) deforming with an initial impact velocity  $V_0$ , and the velocity decreases linearly to zero from the hinge to the beam edge. The initial deflection is zero.

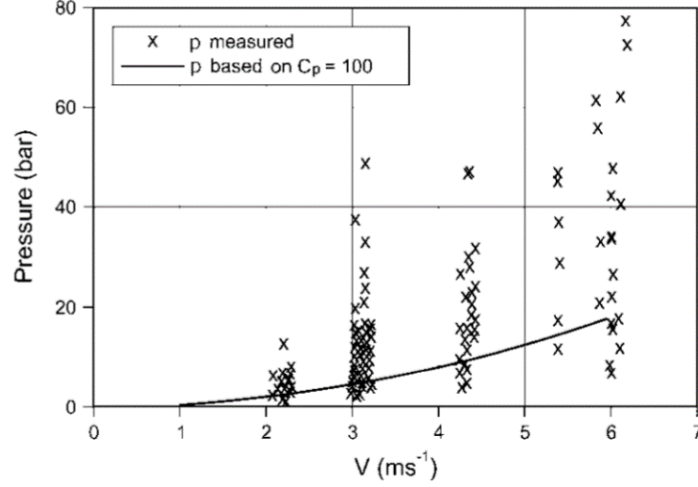


Fig. 4. Measured maximum pressure from different drop tests of the horizontal plates as a function of water entry velocity, from Faltinsen (2005)

In the following, we examine the free-deflection phase to estimate the hydrodynamic pressure acting on the beam. In this phase, there are no excitation loads as the slamming impulse loading in the acoustic stage has died out. Therefore, the only experienced loads are induced by the body deformations. To estimate them, we need to solve a 2D flexible-motion radiation problem using the potential-flow theory. The air effects are neglected. The beam is fully wet and is surrounded by a flat free surface. It means that we neglect the wetness of other parts of the structure to which the beam belongs. This assumption allows an analytical solution of the problem but is an error source in the estimation of added-mass effects. Quantifying the importance of such approximation for the structural response is left for the future.

Assume that the body velocity is equal to the structural deformation mode  $w_{mode}$ , i.e.  $V_m = 1$ . This is consistent with what is done in a rigid-motion radiation problem. We consider the 2D semi-infinite liquid domain in Fig. 5. Within potential-flow theory, the flow caused by the body motion can be solved in terms of a velocity potential,  $\varphi$ . This satisfies the Laplace equation in water:

$$\nabla^2 \varphi = 0 \quad (7)$$

In linear steady-state conditions,  $\varphi$  satisfies the combined free-surface boundary condition:

$$-\omega_b^2 \varphi + g \frac{\partial \varphi}{\partial z} = 0, \quad \text{on } z = 0 \quad (8)$$

on the mean free surface. Here,  $\omega_b$  is the forced oscillation frequency of the body. During slamming, fluid accelerations are much larger than the gravitational acceleration  $g$  in the near field of the body. Therefore, the infinite frequency free-surface condition applies, which is:

$$\varphi = 0, \quad \text{on } z = 0 \quad (9)$$

Along the body, the impermeability condition applies:

$$\frac{\partial \varphi}{\partial z} = w_{\text{mode}}, \quad z = 0, \quad 0 \leq x \leq 2L \quad (10)$$

According to Kvalsvoild and Faltinsen (1995), the solution of this boundary-value problem becomes much simpler if the body-boundary condition is satisfied in an average manner over the beam length, and this yields:

$$\frac{\partial \varphi}{\partial z} = \frac{1}{L} \int_0^L w_{\text{mode}} dx, \quad z = 0, \quad 0 \leq x \leq 2L \quad (11)$$

In the right-hand-side of eq. (11), the beam symmetry has been used when averaging the beam velocity.

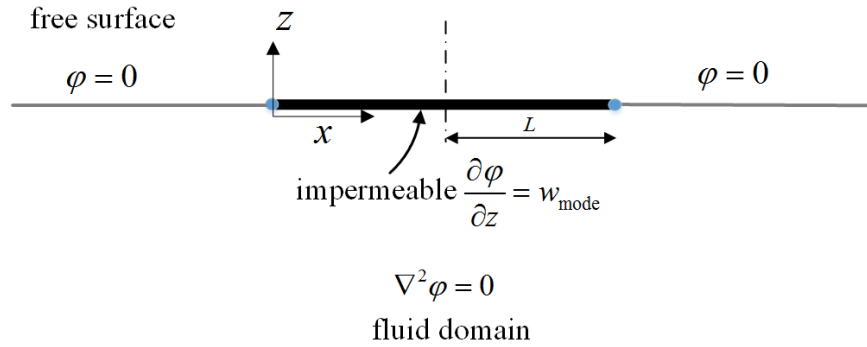


Fig. 5. Boundary value problem for the velocity potential  $\varphi$

The resulting problem corresponds to a rigid-plate heave problem. The solution of the velocity potential on the body is (see e.g. Faltinsen (2005)):

$$\varphi = \frac{1}{L} \int_0^L w_{\text{mode}} dx \cdot \sqrt{L^2 - (L-x)^2}, \quad 0 \leq x \leq 2L, \quad z = 0 \quad (12)$$

From this we can estimate the pressure acting on the body from the Bernoulli's equation. The pressure relative to the atmospheric pressure is:

$$p_\varphi = -\rho g z - \rho \frac{\partial \varphi}{\partial t} - \frac{1}{2} \rho (\nabla \varphi)^2 \quad (13)$$

During slamming, considering the conservation of fluid momentum, the terms associated with fluid accelerations are much higher than those associated with spatial gradients. This makes the time

derivative term dominant over the quadratic term with space derivatives. Moreover, neglecting the hydrostatic term connected with gravity action, the pressure is simplified as  $p_\varphi = -\rho \frac{\partial \varphi}{\partial t}$ . In our original problem, the body velocity was  $V_m(t)w_{\text{mode}}$ . The related velocity potential  $\phi$  is therefore  $\phi = V_m(t)\varphi$  due to the linearity, and the pressure acting on the body is:

$$p = -\rho \dot{V}_m(t)\varphi - \rho V_m(t) \frac{\partial \varphi}{\partial t} \quad (14)$$

Eq. (14) can be applied in stages 1-3 to estimate the pressure. The first pressure term is proportional to the structure acceleration and represents an added-mass effect of the involved structural deformation mode. The second term is connected with added-mass time variation due to changes in the structural deformation mode.

During stage 1 of the free-deflection phase, the structural deformation mode  $w_{\text{mode}}(x, X(t))$  changes in time due to the moving hinges, and the pressure is expressed as:

$$\begin{aligned} p &= -\rho \dot{V}_m(t)\varphi - \rho V_m(t) \frac{\partial \varphi}{\partial X} \dot{X} \\ &= -\frac{2L-X}{2L} \rho \cdot \dot{V}_m(t) \sqrt{L^2 - (L-x)^2} + \frac{1}{2L} \rho V_m(t) \dot{X} \sqrt{L^2 - (L-x)^2}; \quad 0 \leq x \leq 2L, z = 0 \end{aligned} \quad (15)$$

During stages 2 and 3, the structural deformation mode  $w_{\text{mode}}(x)$  does not change in time (refer Fig. 3 and Sections 5.2 and 5.3), and the second pressure term in Eq. (14) vanishes. The pressure becomes,

$$p = -\frac{\rho}{L} \int_0^L w_{\text{mode}}(x) dx \cdot \dot{V}_m(t) \sqrt{L^2 - (L-x)^2}, \quad 0 \leq x \leq 2L, \quad z = 0 \quad (16)$$

No wave making damping forces are induced because the free surface condition  $\varphi = 0$  implies that no radiated waves can be generated on the free surface.

#### 4. Yield functions based on generalized forces

In stages 1 and 2 with travelling and stationary hinges, the beam dissipates energy and decelerates under the action of the bending moment  $M$  and the membrane force  $N$ .  $M$  and  $N$  interact through the yield function and the flow rule.

For beams with rectangular cross sections, the yield function is,

$$F = \frac{M}{M_0} + \left( \frac{N}{N_0} \right)^2 - 1 = 0 \quad (17)$$

where  $M_0 = \frac{1}{4} \sigma_y b h^2$  is the fully plastic bending moment,  $N_0 = \sigma_y b h$  is the fully plastic axial force of the cross section in tension,  $b$  is the beam width and  $h$  is the beam height.

For stiffened panels, Yu et al. (2018) proposed a simplified model for large inelastic deformation resistance with finite axial restraints subjected to lateral loading. The predicted resistance curves showed excellent agreement with those from experiments and numerical simulations when strain hardening was disregarded. Depending on the magnitude of the axial force, the stiffened panel response was classified into four different stages (refer Fig. 6): (R1) tension force in the plate flange only, (R2) tension force in the plate flange and the web, (R3) tension force in the plate flange, the web and the top flange, and (R4) pure tension.

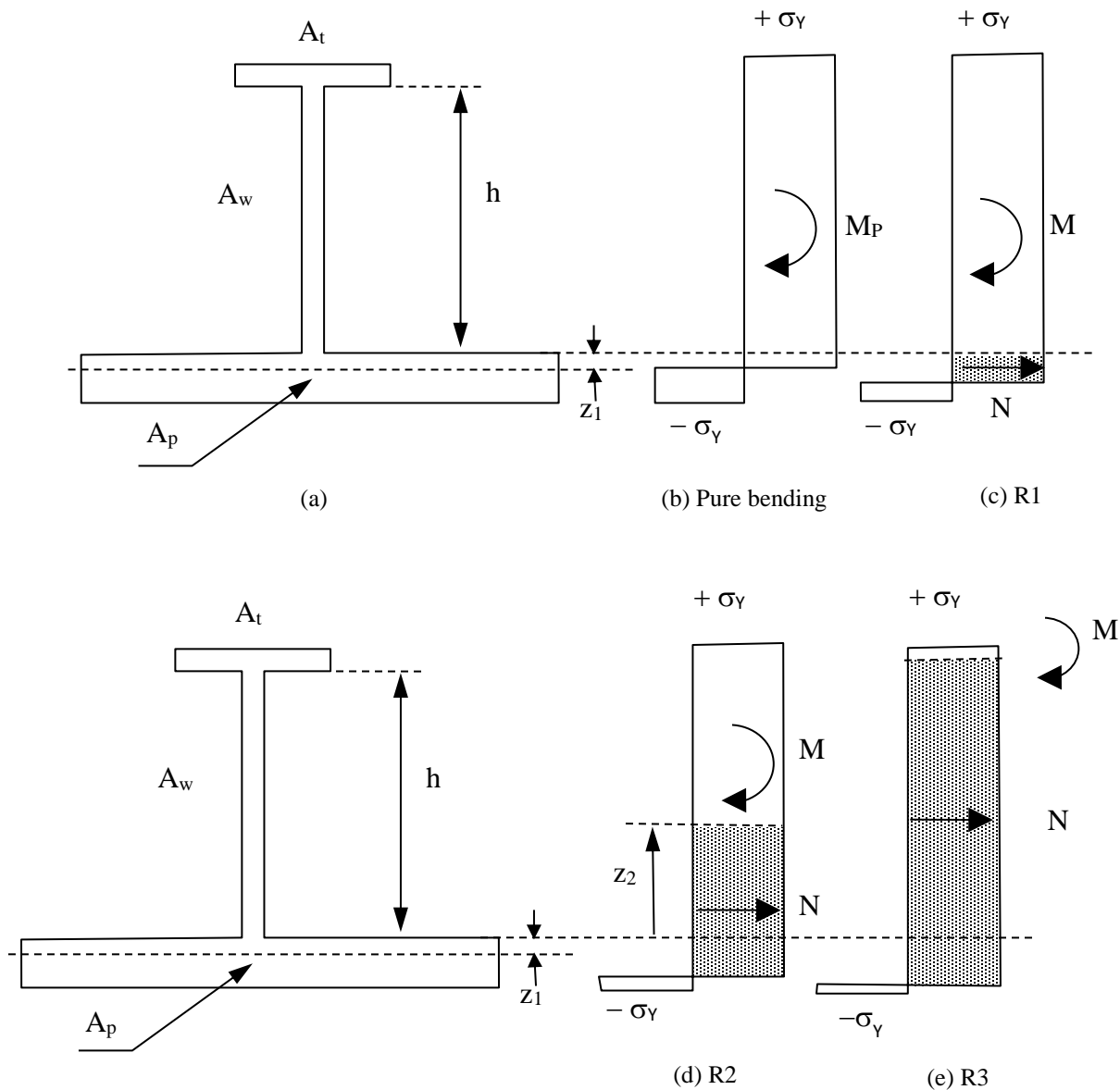


Fig. 6. Evolution of bending moment and axial tension force in stiffened panel cross section, from Yu et al. (2018)

From initial yielding in bending to the pure tension stage, the plastic neutral axial shifts from within the plate flange to the centroid of the cross section. This shift was considered small and negligible. This gives a symmetric yield function with respect to both axes as shown in Fig. 7, and the expressions for the yield functions are as follows:

$$F = \begin{cases} \frac{M}{M_0} - 1 = 0 & \text{stage 1: } 0 < \frac{N}{N_0} < \frac{N^*}{N_0} \\ \frac{M}{M_0} + \frac{1}{1 + 2\frac{A_t}{A_w}} \left( \frac{A_e}{2A_w} \right)^2 \left( \frac{N - N^*}{N_0} \right)^2 - 1 = 0 & \text{stage 2: } \frac{N^*}{N_0} \leq \frac{N}{N_0} \leq \frac{N^{**}}{N_0} \\ \frac{M}{M^{**}} + \frac{N - N^{**}}{N_0 - N^{**}} - 1 = 0 & \text{stage 3: } \frac{N^{**}}{N_0} < \frac{N}{N_0} < 1 \\ \frac{N}{N_0} - 1 = 0 & \text{stage 4} \end{cases} \quad (18)$$

where, the fully plastic bending moment and tension yielding force of the cross section are  $M_0 = \sigma_y \left( A_t h + A_w \frac{h}{2} \right)$ ;  $N_0 = \sigma_y A_e$ , respectively. In eq. (18),  $N^* = \frac{2A_p - A_e}{A_e} N_0$  is the membrane force when the force starts to occupy the web.  $N^{**} = \frac{A_e - 2A_t}{A_e} N_0$  and  $M^{**} = \sigma_y A_t h$  are the membrane force and the bending moment, respectively, when tension forces go into the top flange. The sectional areas  $A_p$ ,  $A_t$  and  $A_w$  are defined in Fig. 6.

According to the analytical model for stiffened panels with fixed ends, stage R1 (axial force in the plate flange only) and stage R3 (axial force in the plate flange, web and top flange) occupy only one point on the resistance-deflection curve, respectively, as shown in Fig. 8. Therefore, only the yield function of stage R2 (axial force in the plate flange and web) needs to be considered for the studied problem before the pure tension stage. This greatly simplifies the problem. However, for stiffened panels with finite axial restraints at the supports, stages R1 and R3 become extended (refer Fig. 8), and should be considered.

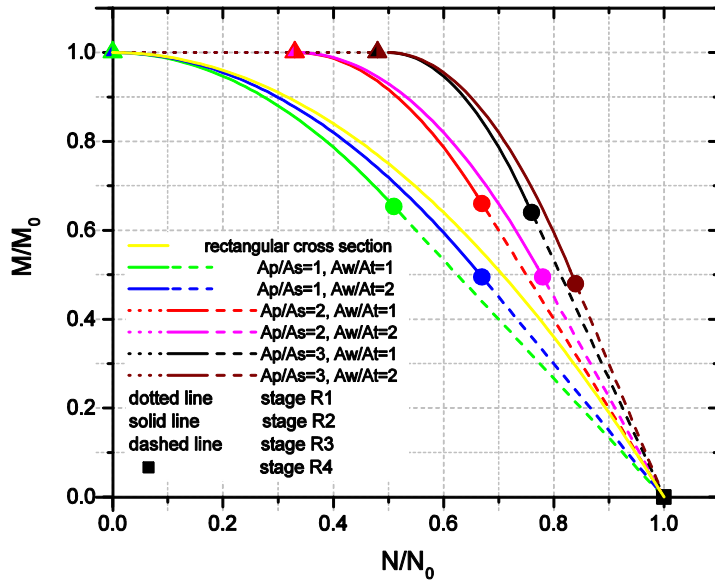


Fig. 7. Yield functions based on force resultants for rectangular beams and stiffened panels

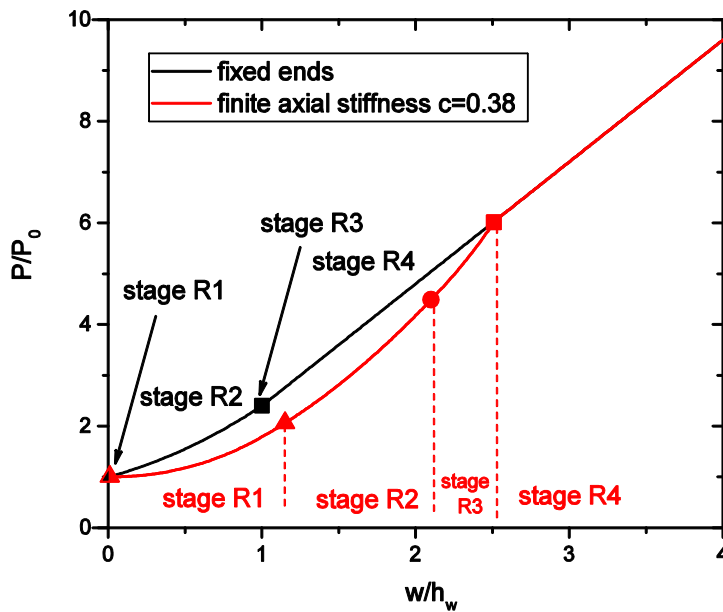


Fig. 8. Force displacement curves of stiffened panels,  $A_p=600 \text{ mm} \times 8 \text{ mm}$ ,  $A_w=180 \text{ mm} \times 10 \text{ mm}$ ,  $A_t=100 \text{ mm} \times 6 \text{ mm}$ , beam length=5 m

Drucker's postulate (the normality criterion) for plastic flow states that the instantaneous virtual elongation rate and rotation rate in the plastic hinges should satisfy:

$$\frac{\dot{\epsilon}}{\dot{\theta}} = \frac{\frac{\partial F}{\partial N}}{\frac{\partial F}{\partial M}} \quad (19)$$

By combining eqs. (6) and (19), the development of bending moment  $M$  and membrane force  $N$  depends on the central deflection  $\delta$ , as given below:

For rectangular beams with fixed ends:

$$\begin{aligned} \frac{N}{N_0} &= \frac{\delta}{h} \\ \frac{M}{M_0} &= 1 - \left(\frac{\delta}{h}\right)^2 \end{aligned} \quad (20)$$

For stiffened panels with fixed ends:

$$\begin{aligned} \frac{N}{N_0} &= \frac{2A_w}{A_e} \frac{\delta}{h} + \frac{2A_p - A_e}{A_e} \\ \frac{M}{M_0} &= 1 - \frac{A_w}{A_w + 2A_t} \left(\frac{\delta}{h}\right)^2 \end{aligned} \quad (21)$$

For fixed boundary conditions, the pure tension stage will be reached when  $\delta = h$ . One should note that Eq. (21) does not give full capacity when  $\delta = h$ . This is because stage R3 represents only one point on the resistance curve (refer to Fig. 8), and the yield status will jump directly from the end of stage R2 to the pure tension stage R4 but still preserving the continuity of resistance curves between different stages. For simply supported beams, pure tension stage is reached when  $\delta = h/2$ .

## 5. Hydro-plastic response of rectangular beams and stiffened panels

Given the information of structural deformation modes from *Section 2*, the hydrodynamic pressure in the free-deflection phase from *Section 3*, and the evolution of bending moments and membrane forces from *Section 4*, we are now ready to examine the hydro-plastic response in the three beam deformation stages.

### 5.1 STAGE 1: TRAVELLING HINGE STAGE

In the travelling hinge stage, the flat central segment  $X(t) \leq x \leq L$  has zero curvature, which yields constant bending moment along the segment and zero shear force at the travelling hinges. It is assumed that hydrodynamic forces mainly concentrate on the rotating side beams. The central portion therefore moves with a constant velocity  $V_m = V_0$  in stage 1, which yields,

$$\delta = V_0 t \quad (22)$$

With  $V_m$  being constant in stage 1, the first term in the pressure expression in Eq. (15) vanishes.

The principle of virtual work applies, which yields:

$$\dot{W}_{\text{external}} = \dot{W}_{\text{internal}} + \dot{W}_{\text{kinetic}} \quad (23)$$

where  $W_{\text{external}}$  is the work done by external forces, i.e. the hydrodynamic forces,  $W_{\text{internal}}$  is the energy dissipated by the beam through deformations, and  $W_{\text{kinetic}}$  is the kinetic energy of the beam.

Considering half of the clamped beam, the work rate of the external force is,

$$\dot{W}_{\text{external}} = \int_0^L p(x)b \cdot v(x, X, t) dx = -\rho b L V_0^2 \dot{X} \int_0^1 \frac{\partial \varphi}{\partial X} \cdot \frac{\partial \varphi}{\partial z} d(x/L) \quad (24)$$

The rate of energy dissipation in the rigid plastic beam is

$$\dot{W}_{\text{internal}} = \sum_{i=1}^n N \dot{e}_i + \sum_{i=1}^n M \dot{\theta}_i = (2M + N\delta) \omega \quad (25)$$

where  $\dot{e}_i$  and  $\dot{\theta}_i$  are the elongation and rotation rate, respectively, at the  $i_{th}$  plastic hinge of the beam. Considering half of the beam, we have two hinges for beams in clamped conditions; thus  $n = 2$ .

In half beam, the rate of change of the kinetic energy has only contribution from  $x < X$  and is:

$$\dot{W}_{\text{kinetic}} = \int_0^L m \dot{w}(x, X, t) \dot{w}(x, X, t) dx = \frac{mX^3 \omega \dot{\omega}}{3} \quad (26)$$

Substituting eqs. (24-26) in eq. (23), we obtain:

$$-\rho b L V_0^2 \dot{X} \int_0^1 \frac{\partial \varphi}{\partial X} \cdot \frac{\partial \varphi}{\partial z} d(x/L) = \frac{mX^3 \dot{\omega} \omega}{3} + (2M + N\delta) \omega \quad (27)$$

According to Fig. 3(a), the following geometric relationship applies,

$$\omega X = V_0 \Rightarrow \dot{\omega} X + \omega \dot{X} = 0 \Rightarrow \dot{\omega} = -\frac{V_0 \dot{X}}{X^2} \quad (28)$$

By substituting eq. (28) into eq. (27) and rearranging the terms, we obtain the governing motion equation for the rate of  $X^2$ :

$$\frac{d(X^2)}{dt} = \frac{2(2M + N\delta)}{\frac{mV_0}{3} - \rho b V_0 L \int_0^1 \frac{\partial \varphi}{\partial X} \cdot \frac{\partial \varphi}{\partial z} d(x/L)} \quad (29)$$

In a non-dimensional format, it reads:



$$\frac{d\left(\frac{X}{L}\right)^2}{d\left(\frac{\delta}{h}\right)} = \frac{1}{\left(V_0\sqrt{\frac{\rho L^3}{M_0 h/b}}\right)^2} \cdot \frac{4\left(\frac{M}{M_0} + \frac{N\delta}{2M_0}\right)}{\frac{m}{3\rho bL} - \underbrace{\int_0^1 \frac{\partial\varphi}{\partial X} \cdot \frac{\partial\varphi}{\partial z} d(x/L)}_{I_A}} \quad (30)$$

Introducing in eq. (30) the simplified solution for  $\varphi$  in eq. (12), the non-dimensional parameter  $I_A$  reads,

$$I_A = \int_0^1 \frac{\partial\varphi}{\partial X} \cdot \frac{\partial\varphi}{\partial z} d(x/L) = -\frac{1}{2} \left( \frac{1}{\left(\frac{X}{L}\right)} \int_0^{\frac{X}{L}} u\sqrt{-u^2+2u} du + \int_{\frac{X}{L}}^1 \sqrt{-u^2+2u} du \right) \quad (31)$$

The integrals in eq. (31) are obtained as:

$$\int_0^{\frac{X}{L}} u\sqrt{-u^2+2u} du = \frac{\pi}{4} - \frac{1}{2} \arcsin\left(1 - \frac{X}{L}\right) - \frac{1}{2} \left(1 - \frac{X}{L}\right) \sqrt{2\frac{X}{L} - \left(\frac{X}{L}\right)^2} - \frac{1}{3} \sqrt{\left(2\frac{X}{L} - \left(\frac{X}{L}\right)^2\right)^3} \quad (32)$$

$$\int_{\frac{X}{L}}^1 \sqrt{-u^2+2u} du = \frac{1}{2} \left[ \arcsin\left(1 - \frac{X}{L}\right) + \left(1 - \frac{X}{L}\right) \cdot \sqrt{2\frac{X}{L} - \left(\frac{X}{L}\right)^2} \right] \quad (33)$$

It can be proved that the term  $\frac{1}{\left(\frac{X}{L}\right)} \int_0^{\frac{X}{L}} u\sqrt{-u^2+2u} du$  in eq. (31) goes to zero when the travelling

hinge gets close to the support.

Eq. (30) is the governing equation for the development of the travelling hinges in stage 1. In order to solve it, the initial condition of  $X$ , i.e.  $X(t=0)$  must be specified. Schubak et al. (1993b) and Jones (2011) found that for beams subjected to a uniform rectangular-shaped impulsive loading with intensity  $q$ , the initial position of travelling hinges is at  $\frac{X(t=0)}{L} = \sqrt{\frac{3q_0}{q}}$ , where  $q_0 = 4M_0/L^2$

is the static collapse load in bending for the beam. In the considered slamming case, the pressure in the acoustic phase may be approximated with a triangular impulse, where the peak pressure is equal to the acoustic pressure (Hagiwara and Yuhara, 1974) given by,

$$P_{acoustic} = \rho c_e V_0 \quad (34)$$

where,  $c_e$  is the speed of sound in water. The triangular pressure in the acoustic phase can be further approximated by a rectangular pressure with the value of half of the acoustic pressure. Therefore, the initial position of the travelling hinge can be expressed as,

$$\frac{X(t=0)}{L} = \sqrt{\frac{24M_0}{\rho c_e V_0 b L^2}} = \sqrt{\frac{24}{\left(V_0 \sqrt{\frac{\rho L^3}{M_0 h/b}}\right)^2} \cdot \frac{V_0 L}{c_e h}} \quad (35)$$

Eq. (35) shows that the initial position of the travelling hinges gets closer to the supports for a larger impact velocity or smaller structural resistance in bending.

According to eqs. (20-21), for the cross section of rectangular beams, we have:

$$\frac{M}{M_0} + \frac{N\delta}{2M_0} = 1 + \frac{\delta^2}{h^2} \quad (36)$$

For stiffened plates, we have

$$\frac{M}{M_0} + \frac{N\delta}{2M_0} = 1 + \frac{A_w}{A_w + 2A_t} \left(\frac{\delta}{h}\right)^2 + \frac{2A_p - A_e}{A_w + 2A_t} \frac{\delta}{h} \quad (36)$$

The right-hand side of eq. (30) is then known and the evolution of traveling hinges in stage 1 can be determined.

### 5.2 STAGE 2: STATIONARY HINGE STAGE

At a certain time instant, say  $t_1$ , the travelling hinges meet in the middle span while  $V_0 t_1 = \delta_1 < h$ . The stationary hinge stage then initiates. The beam middle span velocity  $V_m$  is no longer constant and starts to decrease from  $V_0$ . Combining the work rate balance in eq. (23), and the pressure relationship in eq. (16), we obtain:

$$-\rho b L^3 \dot{V}_m \int_0^1 \frac{\varphi}{L} \frac{\partial \varphi}{\partial z} d\left(\frac{x}{L}\right) = \frac{mL^3}{3} \left(\frac{\dot{V}_m}{L}\right) + (2M + N\delta) \quad (38)$$

As the relation  $\dot{V}_m = \frac{dV_m}{dt} = \frac{dV_m}{d\delta} \cdot \frac{d\delta}{dt} = \frac{dV_m}{d\delta} V_m$  applies, eq. (38) becomes:

$$\begin{aligned} V_m dV_m \left[ -\rho b L^3 \int_0^1 \frac{\varphi}{L} \frac{\partial \varphi}{\partial z} d\left(\frac{x}{L}\right) - \frac{mL^2}{3} \right] &= (2M + N\delta) d\delta \\ V_m^2 \left[ -\rho b L^3 \int_0^1 \frac{\varphi}{L} \frac{\partial \varphi}{\partial z} d\left(\frac{x}{L}\right) - \frac{mL^2}{3} \right] &= 2 \int_0^{\delta} (2M + N\delta) d\delta + C_1 \end{aligned} \quad (39)$$

where  $C_1$  is an integration constant that should be determined based on the continuity of the displacement at the end of stage 1 with that at the beginning of stage 2:

$$C_1 = V_0^2 \left[ -\rho b L^3 \int_0^1 \frac{\varphi}{L} \frac{\partial \varphi}{\partial z} d\left(\frac{x}{L}\right) - \frac{mL^2}{3} \right] - 2 \int_0^{\delta_1} (2M + N\delta) d\delta \quad (40)$$

The integrals on the right hand side of eqs (39-40) can be calculated. Thus, for rectangular beams, the midspan deflection is solved from eq. (39):

$$\frac{d\delta}{dt} = \sqrt{\frac{4M_0 \left( \delta + \frac{\delta^3}{3h^2} \right) + C_1}{-\rho b L^3 \int_0^1 \frac{\varphi}{L} \frac{\partial \varphi}{\partial z} d\left(\frac{x}{L}\right) - \frac{mL^2}{3}}} \quad (41)$$

In a non-dimensional format, it reads:

$$\frac{V_m}{V_0} = \sqrt{\frac{1}{\left( V_0 \sqrt{\frac{\rho L^3}{M_0 h / b}} \right)^2} \cdot \frac{4 \left( \frac{\delta}{h} + \frac{1}{3} \left( \frac{\delta}{h} \right)^3 \right) + \frac{C_1}{M_0 h}}{\left[ \underbrace{-\int_0^1 \frac{\varphi}{L} \frac{\partial \varphi}{\partial z} d\left(\frac{x}{L}\right)}_{I_B} - \frac{m}{3\rho b L} \right]}}} \quad (42)$$

For stiffened panels, we obtain:

$$\frac{d\delta}{dt} = \sqrt{\frac{4M_0 \left( \delta + \frac{A_w \delta^3}{3(A_w + 2A_t)h^2} + \frac{(2A_p - A_e)\delta^2}{2(A_w + 2A_t)h} \right) + C_1}{\left[ -\rho b L^3 \int_0^1 \frac{\varphi}{L} \frac{\partial \varphi}{\partial z} d\left(\frac{x}{L}\right) - \frac{mL^2}{3} \right]}}} \quad (43)$$

which, in non-dimensional format, reads:

$$\frac{V_m}{V_0} = \sqrt{\frac{1}{\left( V_0 \sqrt{\frac{\rho L^3}{M_0 h / b}} \right)^2} \cdot \frac{4 \left( \frac{\delta}{h} + \frac{A_w}{3(A_w + 2A_t)} \left( \frac{\delta}{h} \right)^3 + \frac{(2A_p - A_e)}{2(A_w + 2A_t)} \left( \frac{\delta}{h} \right)^2 \right) + \frac{C_1}{M_0 h}}{\left[ \underbrace{-\int_0^1 \frac{\varphi}{L} \frac{\partial \varphi}{\partial z} d\left(\frac{x}{L}\right)}_{I_B} - \frac{m}{3\rho b L} \right]}}} \quad (44)$$

Based on the simplified solution in eq. (12), when  $X = L$ , the non-dimensional parameter  $I_B$  is

$$I_B = \int_0^1 \frac{\varphi}{L} \frac{\partial \varphi}{\partial z} d\left(\frac{x}{L}\right) = \frac{1}{2} \int_0^1 u \sqrt{-u^2 + 2u} du = \frac{1}{2} \left( \frac{\pi}{4} - \frac{1}{3} \right) \quad (45)$$

The right-hand sides of eqs. (42) and (44) are then known and the evolution of  $\delta$  in stage 2 can be determined.

### 5.3 STAGE 3: PURE TENSION STAGE

When the central deflection reaches  $\delta = h$  for beams with fixed ends, the beam bending moment will decrease to zero and the whole cross section will be occupied by the yield membrane forces  $N_0$ . The pure tension stage 3 may be reached in two paths, from either stage 2 or directly from stage 1 as shown in Fig. 9.

- **Path 1**

In the cases where stage 1 ends with the travelling hinges merged in the beam middle span and  $V_0 t_1 = \delta_1 < h$ , stage 2 starts and deflection continues. At time  $t_2$ , when the central deflection reaches the beam height, i.e.  $\delta_2 = h$  while the velocity has not decreased to zero i.e.  $V_m > 0$ , stage 3 initiates. This is often the case for thick beams, e.g. stiffened panels.

- **Path 2**

In cases with thin plates, stage 1 ends at time  $t'_1$  with the beam central deflection reaching the beam height, i.e.  $\delta'_1 = V_0 t'_1 = h$ , while the hinges have not travelled to the middle span, i.e.  $X \leq L$ .

At the beginning of stage 3, say at time  $t_3$ , there is a sudden change of the deformation mode and the deflection velocity, i.e.  $V_m(t_3^-) \neq V_m(t_3^+)$ . By holding the central deflection  $\delta$  constant and equating the kinetic energy through the transition, we obtain the following relationship between the velocity before and after the start of stage 3, respectively,  $V_m(t_3^-)$  and  $V_m(t_3^+)$ :

$$V_m(t_3^+) = V_m(t_3^-) \sqrt{2 - \frac{4X}{3L}} \quad (46)$$

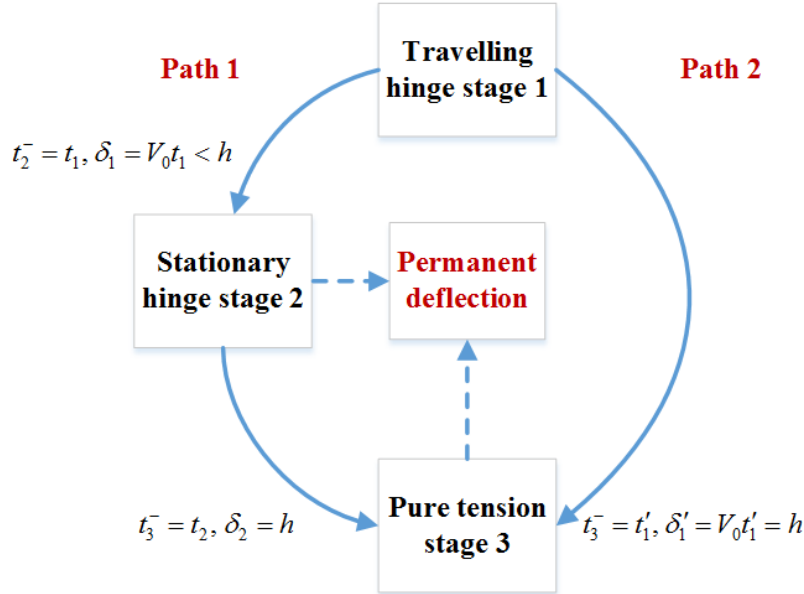


Fig. 9. Response of beams during the free-deflection phase initiated by impulsive loading

In the pure tension stage, the beam behaves as a plastic string with the following equation of motion:

$$m \frac{\partial^2 w}{\partial t^2} - N_0 \frac{\partial w^2}{\partial x^2} = p(x, w, t) b \quad (47)$$

The pressure  $p$  on the right hand side of eq. (47) is a function of the beam deflection  $w$ . Here, the problem is solved expressing the displacement  $w$  in terms of the beam dry normal modes,  $\psi_n$ , within a modal approach:

$$w(x, t) = \sum_{n=1}^{\infty} A_n(t) \cdot \psi_n(x) \quad (48)$$

with unknown coefficients  $A_n$ . The dry normal modes are a good approximation of the wet normal modes when the added mass distribution is similar to the mass distribution (see e.g. Faltinsen (2005)). The dry modes can be found by substituting eq. (48) in eq. (47) and setting  $p = 0$ . Assuming steady-state oscillations, each coefficient  $A_n$  will be in the form  $e^{i\omega_{n,dry}t}$ , with  $\omega_{n,dry}$  the dry natural frequency associated with the  $n_{th}$  eigenmode  $\psi_n$ . This gives:

$$-\omega_{n,dry}^2 \psi_n - \frac{N_0}{m} \psi_{n,xx} = 0 \quad (49)$$

The solution of eq. (49) can be expressed as:

$$\psi_n = B_n \sin\left(\omega_{n,dry} \sqrt{\frac{m}{N_0}} x\right) + D_n \cos\left(\omega_{n,dry} \sqrt{\frac{m}{N_0}} x\right); \quad n = 1, 2, 3, \dots \quad (50)$$

The boundary conditions of  $\psi_n(0) = \psi_n(2L) = 0$  implies  $D_n = 0$ , and we obtain:

$$\begin{aligned} \psi_n &= B_n \sin\left(\omega_{n,dry} \sqrt{\frac{m}{N_0}} x\right) \\ \omega_{n,dry} \sqrt{\frac{m}{N_0}} 2L &= n\pi, \quad n = 1, 2, 3, \dots \end{aligned} \quad (51)$$

Experiments on water-entry of flat plates from Shin et al. (2017) show that the first mode shape dominates the permanent beam deflections. Therefore, only the first mode is considered. This gives:

$$\omega_{1,dry} = \frac{\pi}{2L} \sqrt{\frac{N_0}{m}} \quad (52)$$

The beam deflection can then be expressed as:

$$w(x, t) = A_1(t) \sin\left(\frac{\pi x}{2L}\right) \quad (53)$$

Thus,  $w_{\text{mode}}(x) = \sin \frac{\pi x}{2L}$  in *stage 3*, and using eq. (16) the pressure acting on the beam can be expressed as:

$$p = -\frac{2}{\pi} \rho \ddot{A}_1(t) \sqrt{(L^2 - (L-x)^2)} \quad (54)$$

By substituting eq. (54) into eq. (47), we obtain:

$$m \ddot{A}_1(t) \cdot \sin \frac{\pi x}{2L} + \frac{\pi^2}{4L^2} N_0 A_1(t) \sin \frac{\pi x}{2L} = -\frac{2}{\pi} \rho b \ddot{A}_1(t) \sqrt{(L^2 - (L-x)^2)} \quad (55)$$

Eq. (55) depends on both  $x$  and  $t$ . In order to determine  $A_1(t)$ , we follow the standard solution technique within a modal approach. We multiply both sides of eq. (55) with the normal mode  $\sin \frac{\pi x}{2L}$  and integrate between 0 and  $L$ . This corresponds to the projection of eq. (55) along this mode. The final equation is expressed as:

$$(M_s + M_a) \frac{d^2 A_1}{dt^2} + K A_1 = 0 \quad (56)$$

Here,  $M_s$  is the generalized structural mass:

$$M_s = m \int_0^L \left( \sin \frac{\pi x}{2L} \right)^2 dx = \frac{mL}{2} \quad (57)$$

$M_a$  is the generalized added mass,

$$M_a = \frac{2}{\pi} \rho b \int_0^L \sqrt{L^2 - (L-x)^2} \cdot \sin \frac{\pi x}{2L} dx = \frac{2}{\pi} \rho b L^2 \int_0^1 \sqrt{2u - u^2} \cdot \sin \left( \frac{\pi}{2} u \right) du \quad (58)$$

and  $K$  is the generalized restoring stiffness,

$$K = \frac{\pi^2}{4L^2} N_0 \int_0^L \left( \sin \frac{\pi x}{2L} \right)^2 dx = \frac{\pi^2 N_0}{8L} \quad (59)$$

The solution of Eq. (56) is expressed as:

$$A_1(t) = C_2 \sin(\omega_{1,\text{wet}} t + \theta) \quad (60)$$

where  $C_2$  and  $\theta$  are constants that denote the amplitude and initial phase of the motion, respectively.  $\omega_{1,\text{wet}}$  is the wet natural frequency of the first eigenmode,

$$\omega_{1,wet} = \sqrt{\frac{K}{M_s + M_a}} \quad (61)$$

Taking the starting time of stage 3 as  $t' = 0$ . The following initial conditions should be satisfied,

$$\begin{aligned} A_1(t' = 0) &= h \\ \frac{dA_1}{dt}(t' = 0) &= V_m(t_3^+) \end{aligned} \quad (62)$$

This yields:

$$\begin{aligned} \frac{C_2}{h} &= \sqrt{\frac{V_m(t_3^+)^2}{\omega_{1,wet}^2 h^2} + 1} \\ &= \sqrt{\left[ \frac{4}{\pi^2} \frac{m}{\rho b L} + \frac{16}{\pi^3} \left( \int_0^1 \sqrt{2u - u^2} \sin\left(\frac{\pi}{2} u\right) du \right) \right] \left[ \left( \frac{V_m(t_3^+)}{V_0} \right)^2 \left( V_0 \sqrt{\frac{\rho L^3}{M_0 h / b}} \right)^2 \left( \frac{M_0}{N_0 h} \right) + 1 \right]} \quad (63) \\ \theta &= \arcsin \frac{1}{\sqrt{1 + \frac{V_m(t_3^+)^2}{\omega_{1,wet}^2 h^2}}} \end{aligned}$$

## 6. Theoretical results

Due to the complexities of the governing equations of the present model, closed-form analytical solutions are difficult to obtain. Thus, the fourth order Runge-Kutta method is adopted to solve the equations numerically. The resulting response of beams and stiffened panels, and parameters that govern the hydro-plastic slamming phenomenon, are discussed in detail.

### 6.1 Hydro-plastic slamming response of plate strips

Plate strips normally have large length-to-thickness ratios such that they often reach their full tension capacity before the hinges have travelled to the middle span. Thus they normally follow Path 2. For very thick plates, stages 1 and 2 may become important, but then they are, of course, also considerably more resistant to slamming loads. According to the analytical model, three non-dimensional parameters are identified:

- The non-dimensional velocity  $V_{0,nd} = V_0 \sqrt{\frac{\rho L^3}{M_0 h / b}} = 2V_0 \sqrt{\frac{\rho}{\sigma_y} \left( \frac{L}{h} \right)^3}$
- The non-dimensional mass  $m_{nd} = m / \rho b L$ , hereafter indicated also as the mass ratio

- The ratio of the initial travelling hinge position relative to half of the beam length

$$X_{nd} = \frac{X(t=0)}{L} = \sqrt{\frac{24}{\left(V_0 \sqrt{\frac{\rho L^3}{M_0 h / b}}\right)^2} \cdot \frac{V_0 L}{c_e h}}$$

Fig. 10 shows the plate strip deflections versus time in a non-dimensional format for different velocities. The mass ratio is kept constant as  $m_{nd} = 0.153$ . The plots show that the non-dimensional velocity  $V_{0,nd}$  is dominant in determining the permanent deflection of a plate strip. Permanent deflection increases significantly with the non-dimensional velocity.

As the plate thickness is normally considerably smaller than the stiffener spacing, the permanent deflection can be many times larger than the plate thickness, and the deflection is mainly governed by stage 3 and follows Path 2. From the expressions of the non-dimensional parameters, it seems difficult to satisfy similarity of the non-dimensional parameters  $V_{0,nd}$  and  $X_{nd}$  simultaneously during scaling. However, the  $X_{nd}$  ratio is only connected with stage 1, and the influence is minor on the permanent deflections.

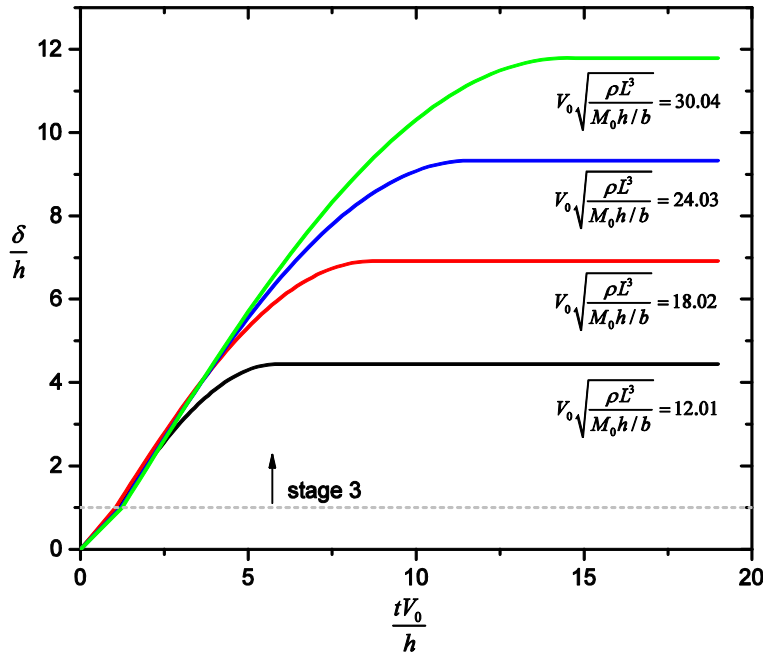


Fig. 10. Non-dimensional time-deflection curves for plate strips with different non-dimensional velocities. The non-dimensional mass ratio is  $m / \rho b L = 0.153$

Next, we examine the importance of the mass ratio  $m_{nd}$ . Fig. 11 plots the non-dimensional curves of panel permanent deflections versus non-dimensional velocity for different mass ratios. Results



show that  $\delta_p / h$  increases significantly with the non-dimensional velocity, and the relationship is virtually linear for large non-dimensional velocities. It is observed that a larger mass ratio  $m / \rho b L$  will lead to larger permanent deflections with the same non-dimensional velocity. This is because the structure is imparted a velocity  $V_0$  in the middle portion regardless of the structural mass. This means that a structure with a larger mass is imparted more kinetic energy, leading to a larger deflection. The variation of the permanent deflection with the mass ratio is however, not significant. For typical steel stiffened panels, the mass ratios are small (added mass predominates) and in the range of 0.1-0.2. Curves in Fig. 11 may be used as basis for designing plates subjected to extreme slamming.

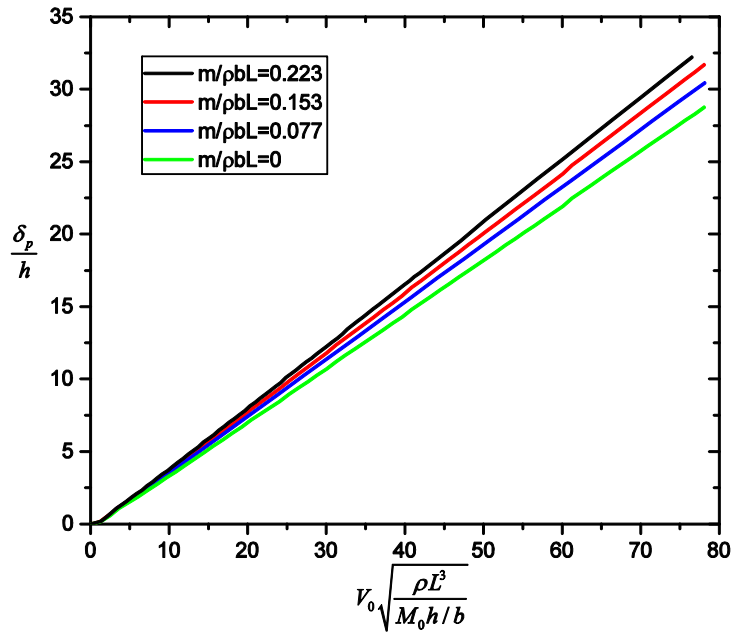


Fig. 11. Non-dimensional permanent deflection versus non-dimensional velocity curves for plate strips with different mass ratios

### 6.2 Hydro-plastic slamming response of stiffened panels

Stiffened panels are characterized by large web heights. The frame spacing/web height ratio is considerably smaller than the stiffener spacing/plate thickness ratio, and thus the deformation is mainly governed by the travelling hinge and stationary hinge stages, where bending and membrane forces interact. Panels with relatively weak stiffeners or panels subjected to extreme slamming loads may also be pushed into the pure tensile membrane stage. According to the analytical model, five non-dimensional parameters are identified:

- The non-dimensional velocity  $V_{0,nd} = V_0 \sqrt{\frac{\rho L^3}{M_0 h / b}}$
- The area ratios  $A_{ps,nd} = A_p / A_s$  and  $A_{wt,nd} = A_w / A_t$
- The non-dimensional mass  $m_{nd} = m / \rho b L$

- The ratio of the initial travelling hinge position relative to the beam half length

$$X_{nd} = \frac{X(t=0)}{L} = \sqrt{\frac{24}{\left(V_0 \sqrt{\frac{\rho L^3}{M_0 h/b}}\right)^2} \cdot \frac{V_0 L}{c_e h}}$$

Fig. 12 shows the non-dimensional panel deflections versus time for different non-dimensional velocities. The area ratios and the mass ratio are kept constant, being  $A_{ps,nd} = 2$ ;  $A_{wt,nd} = 2$  and  $m_{nd} = 0.0919$ . The results show that the non-dimensional velocity  $V_{0,nd}$  is a crucial parameter in determining the permanent deflection. As  $V_{0,nd}$  increases, the deflection  $\delta/h$  and the non-dimensional time  $tV_0/h$  increase significantly. Because of the large web height over length ratios, the typical range of the non-dimensional velocity is much smaller compared to that for plates. Depending on the magnitude of  $V_{0,nd}$ , stiffened panels may go through Path 1 (including only stages 1 and 2 or all the three stages) or Path 2 (including only stages 1 and 3). The non-dimensional curves coincide generally in stage 1.

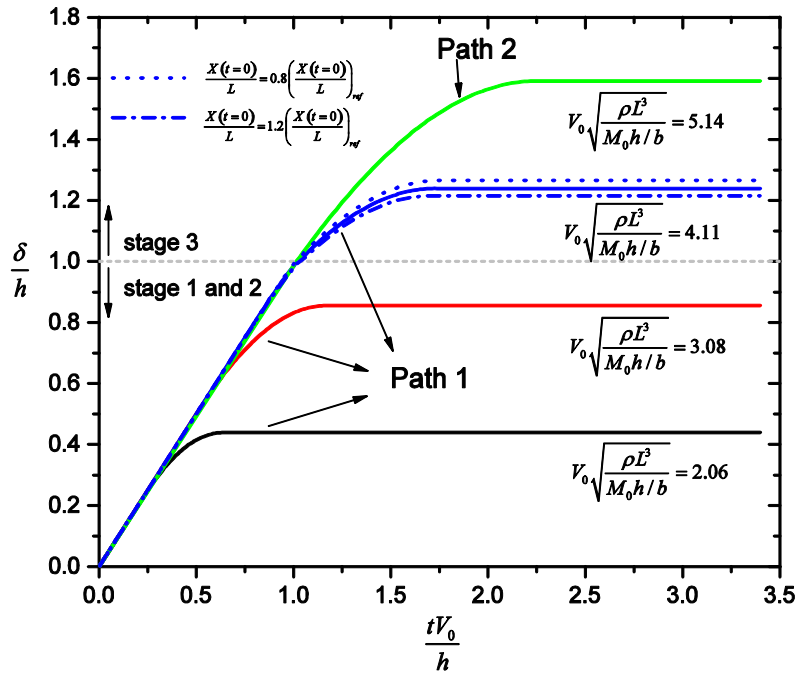


Fig. 12. Non-dimensional time-deflection curves for stiffened panels with different non-dimensional velocities. The area ratios are  $A_p/A_s=2$ ,  $A_w/A_t=2$ , and the non-dimensional mass is  $m / \rho bL = 0.0919$ . The length over height ratio is  $L/h=12.5$

Similar to the situations of plate strips, it is difficult to satisfy the similarity of  $V_{0,nd}$  and  $X_{nd}$  simultaneously during scaling. By keeping the crucial parameter  $V_{0,nd}$  constant, it is interesting to

know how  $X_{nd}$  varies for typical stiffened panels and how much the variation of  $X_{nd}$  influences the predicted permanent deflection. To shed light on this, it is convenient to introduce a reference value  $\left(\frac{X(t=0)}{L}\right)_{ref}$ , and any change relative to this reference value for a specific value of the non-dimensional velocity is expressed as:

$$\frac{X(t=0)/L}{\left(X(t=0)/L\right)_{ref}} = \sqrt{\frac{V_0}{V_{0,ref}} \cdot \frac{L/h}{(L/h)_{ref}}} \quad (64)$$

For stiffened panels, the length over stiffener height ratio is typically in the range of  $10 \leq 2L/h \leq 20$ . Suppose that  $h$  equals  $h_{ref}$  and that  $\left(\frac{2L}{h}\right)_{ref} = 12.5$ . It means  $0.8 \leq L/L_{ref} \leq 1.6$ .

By holding constant the non-dimensional velocity, we obtain the following range for the absolute velocity  $\frac{1}{\sqrt[4]{1.6^3}} \leq V_0/(V_0)_{ref} \leq \frac{1}{\sqrt[4]{0.8^3}}$ . Therefore, the variation of the initial travelling hinge position

for a given non-dimensional velocity ranges as  $0.89 \approx \frac{1}{\sqrt[4]{1.6}} \leq \frac{X(t=0)/L}{\left(X(t=0)/L\right)_{ref}} \leq \frac{1}{\sqrt[4]{0.8}} \approx 1.06$ . Fig.

12 shows the variation of the normalized deflection when  $V_0 \sqrt{\frac{\rho L^3}{M_0 h/b}} = 4.11$  and  $\frac{X(t=0)/L}{\left(X(t=0)/L\right)_{ref}}$

is conservatively set equal to 0.8 and 1.2, respectively. The curves show that the permanent deflection variations are quite small and can be neglected. We therefore adopt a reference value of  $\left(\frac{2L}{h}\right)_{ref} = 12.5$  for the non-dimensional curves below.

Fig. 13 shows the normalized permanent deflection versus the non-dimensional velocity for different mass ratios. The area ratios are  $A_{ps,nd} = 2$ ;  $A_{wt,nd} = 2$ . The permanent deflection increases significantly with increasing non-dimensional velocity. The relationship is non-linear when the deformation is governed by stage 1 and 2, and becomes virtually linear when entering stage 3. The permanent deflections increases with increasing mass ratio  $m_{nd}$ , but the increase is generally limited for the range of interest. The mass ratio is typically small, and it is reasonable to select a representative mass ratio for design purposes.

Fig. 14 displays the normalized permanent deflection versus the non-dimensional velocity for different area ratios of  $A_{ps,nd}$  and  $A_{wt,nd}$ . It shows that the permanent deflection increases with decreasing  $A_{ps,nd}$  and  $A_{wt,nd}$  ratios, and notably the  $A_{ps,nd}$  ratio is dominant. Fig. 14 is well suited to be used as basis for design curves of stiffened panels against extreme water slamming. It is also noticed that the large deflection range ( $\delta_p/h > 1$ ) is often hypothetical because fracture due to excessive straining, local buckling/tripping or shear failure will occur at finite deformations.

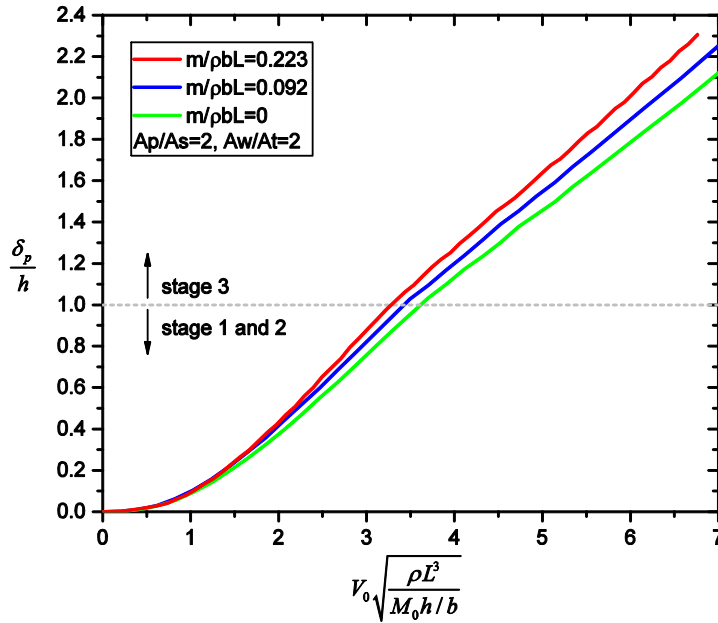


Fig. 13. Non-dimensional permanent deflection versus non-dimensional velocity curves for stiffened panels with different mass ratios. The area ratios are  $A_p/A_s=2$ ,  $A_w/A_t=2$

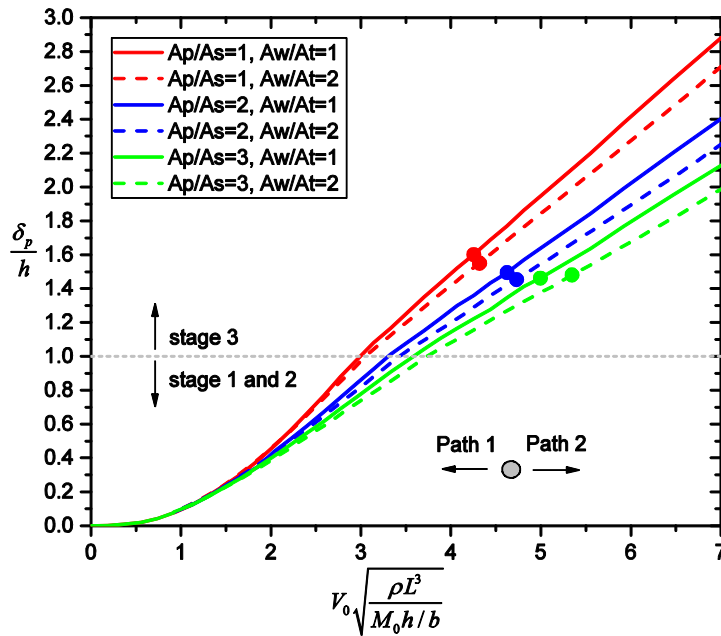


Fig. 14. Non-dimensional permanent deflection versus non-dimensional velocity curves for stiffened panels given different area ratios. The non-dimensional mass is  $m/\rho bL=0.0919$ , and the length over height ratio is  $2L/h=12.5$ . The full circle indicates the limit for Path occurrence, i.e. Path 1 is followed on the left of the circle, while Path 2 is followed on the right

## 7. Discussion

### 7.1 The hydrodynamic part of the model

The analytical model is developed for the fluid-structure interaction in 2D conditions. In practice, the length-to-width ratio may not be large enough to enable a true 2D condition, and the 3D effect on the hydrodynamic pressure may become important. However, because the added mass in a 3D condition is smaller than that in a 2D condition, permanent deflections are smaller in 3D conditions. This can be reflected in rules from DNV (2014), where a correction factor  $C_A$  for the added mass of a heaving flat plate is introduced to account for the 3D effect based on analytical solutions as shown in Fig. 15. Therefore, it is conservative to use 2D solutions for structural design.

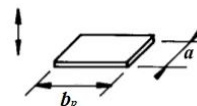
Rectangular plates 	Vertical	$b_p/a$	$C_A$	$b_p/a$	$C_A$
		1.00	0.579	3.17	0.840
1.25	0.642	4.00	0.872		
1.50	0.690	5.00	0.897		
1.59	0.704	6.25	0.917		
2.00	0.757	8.00	0.934		
2.50	0.801	10.00	0.947		
3.00	0.830	$\infty$	1.000		

Fig. 15. The  $C_A$  factor for the added mass of a heaving plate to account for the 3D effect (DNV, 2014)

The hydrodynamic pressure is calculated based on the assumption that the impermeability body-boundary condition is satisfied in an average manner over the length as expressed in eq. (11). In order to assess quantitatively the influence of this assumption, the boundary value problem sketched in Fig. 5 is solved numerically using a 2D Boundary Element Method (BEM) satisfying the exact impermeability condition as expressed in eq. (10). A brief description of the BEM code is given in the *appendix*, and more details can be found in Greco et al. (2004).

Fig. 16 compares the non-dimensional hydrodynamic parameters  $I_A$  and  $I_B$  obtained using the simplified theoretical solution and numerical results from the BEM, where  $I_A$  and  $I_B$  are the crucial parameters from the governing motion eqs. (30), (42) and (44). The results show that for the  $I_A$  parameter, the values differ greatly for small  $X/L$  ratios but become close when  $X/L \geq 0.4$ . Because the initial position of the hinges  $X(t=0)/L$  is non-zero in practice, the influence of  $I_A$  value differences in small  $X/L$  regions is expected to be limited. For the  $I_B$  parameter, the two curves show same behaviors and the values by the numerical code are slightly larger than those by the simplified theoretical method. In order to assess how differences in the values of  $I_A$  and  $I_B$  predicted by the two methods influence the permanent deflections, the  $I_A$  parameter obtained using the BEM results is fitted by polynomials as:

$$\begin{aligned}
 I_A = \int_0^1 \frac{\partial \varphi}{\partial X} \cdot \frac{\partial \varphi}{\partial z} d(x/L) \approx & 9.7834(x/L)^6 - 32.851(x/L)^5 \\
 & + 43.431(x/L)^4 - 28.784(x/L)^3 + 10.373(x/L)^2 - 2.2097(x/L) - 0.0175
 \end{aligned} \tag{65}$$

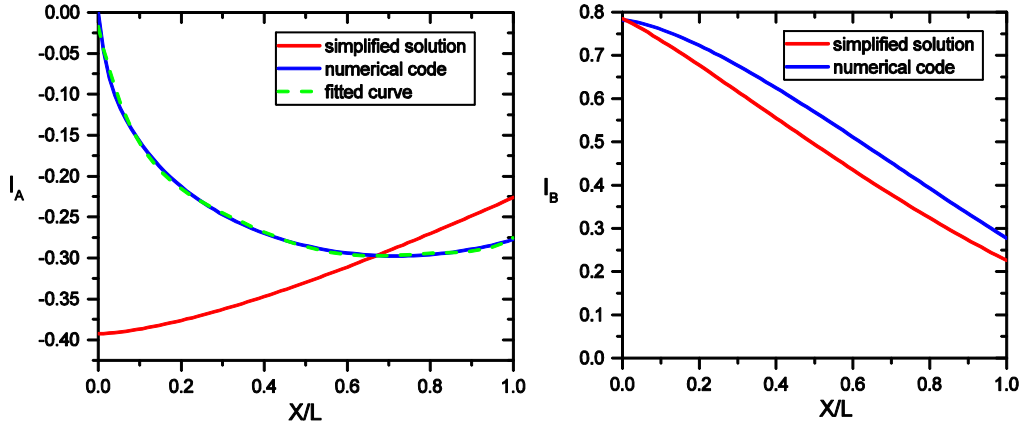


Fig. 16. Comparison of the non-dimensional parameters  $I_A$  and  $I_B$  for hydrodynamics with the BEM and the simplified analytical solution

Fig. 17 compares non-dimensional curves of stiffened-panel deflections versus time with different  $V_{0,nd}$  values predicted by both methods.

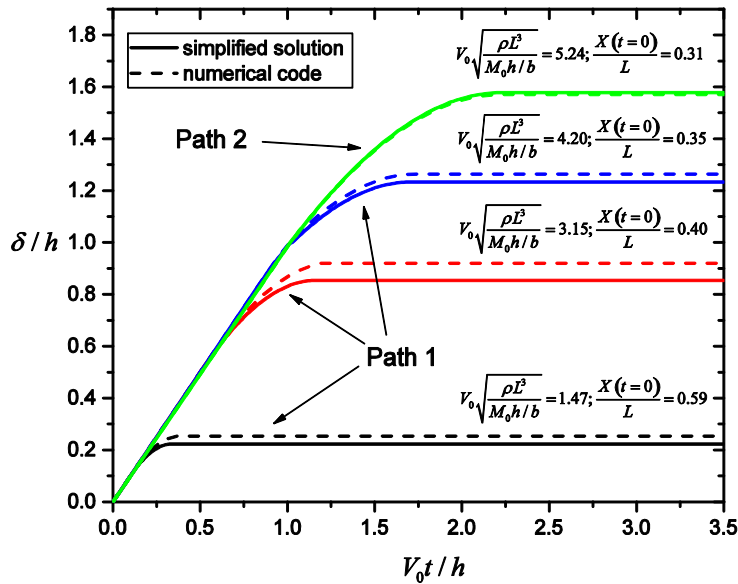


Fig. 17. Deflections of stiffened panels with the hydrodynamics from the BEM and from the simplified analytical solution. The area ratios of the stiffened panels are  $A_p/A_s=2.4$ ,  $A_w/A_t=1.5$ , and the non-dimensional mass is  $m/\rho bL=0.11$ . The length over height ratio is  $2L/h=13.3$

The area ratios of the considered stiffened panels are  $A_p/A_s=2.4$ ,  $A_w/A_t=1.5$ , and the non-dimensional mass is  $m/\rho bL=0.11$ . The length over height ratio is  $2L/h=13.3$ . The results show that the curves from the two approaches are generally close, and that the model using the simplified solution predicts slightly smaller permanent deflections. It is interesting to find that the largest

difference occurs for intermediate  $V_{0,nd}$  values. This is because the total deflection difference has contributions from both stage 1 and stage 2. The  $I_A$  value for stage 1 from BEM can be smaller or larger depending on the  $X/L$  ratios, while the  $I_B$  value for stage 2 from BEM is always larger. The difference is however small, and can generally be neglected.

### 7.2 Discussion of the analytical model

Theoretical analysis has shown that the non-dimensional velocity  $V_0\sqrt{\rho L^3/(M_0 h/b)}$  is dominant in determining the permanent deflections of plates and stiffened panels subjected to extreme water slamming, while the influence of the mass ratio  $m/\rho bL$  is limited. Faltinsen (2005) investigated hydro-elastic slamming of flat beams and found that  $V_0\sqrt{\rho L^3/(EI/b)}$  was a crucial parameter to determine the maximum elastic deflection. It is interesting to find that the non-dimensional velocity for hydro-plastic slamming is consistent with that defined by Faltinsen (2005) for hydroelastic slamming, and the difference is the expression regarding structural stiffness.

Deflections of stiffened panels are mainly governed by the travelling hinge stage and the stationary hinge stage, where permanent deflections increase nonlinearly with the non-dimensional impact velocity according to Fig. 14. For plate strips, the deflections are governed by the pure tensile membrane stage, where permanent deflections are virtually linearly dependent on the non-dimensional velocity. This is similar to the findings by Faltinsen (2005), who showed that the maximum elastic deflection of beams subjected to slamming increased linearly with the non-dimensional velocity  $V_0\sqrt{\rho L^3/(EI/b)}$ .

The typical range of the non-dimensional velocity is quite different for plate strips and stiffened panels because of the large difference in the length over web height ratio. According to Fig. 14, for stiffened-panel permanent deflection up to 3 times the web height, the non-dimensional velocity is typically up to 7. Plate strips have smaller thicknesses and large length over thickness ratios. When subjected to slamming, permanent deflections of plate strips can be many times larger than the plate thickness. According to Fig. 11, for permanent deflections up to 35 times the plate thickness, the non-dimensional velocity may be up to 80.

It should be noted that it is assumed that the elastic energy is small compared to the plastic energy and all kinetic energy is absorbed by plastic deformations. This is generally reasonable for cases with large non-dimensional velocities. When the non-dimensional velocity is small, the elastic deformations become important and the hydro-elastic slamming theory by Faltinsen (2005) should be adopted. In addition, the analytical model assumes the beam response with a travelling hinge mechanism, and the initial position of the travelling hinge is  $X(t=0)/L$  according to eq. (35). In order to activate a travelling hinge mechanism, the condition of  $X(t=0)/L \leq 1$  should be satisfied, and this yields:

$$V_0 \geq \sqrt{\frac{24M_0}{\rho c_e b L^2}} \quad (66)$$

DNV rules stated that ships and offshore structures should be designed to resist loads with an annual probability of  $10^{-2}$  in the Ultimate Limit State (ULS) and an annual probability of  $10^{-4}$  in the Accidental Limit State (ALS) (DNV, 2001). Rules and standards for the design of structures against extreme slamming conditions are however, very few. In 2016, DNV introduced the first rules i.e. DNVGL-OTG-13 (2016) and DNVGL-OTG-14 (2016), for the design of offshore structures against extreme slamming loads in the ULS as a response to the *COSL Innovator* platform accident in the North Sea. The rules suggest a design pressure history where the peak value is no less than 0.4 MPa for ULS design. These provisions neglect, however, the coupling between the fluid and structure deformations. The proposed analytical model results in curves of non-dimensional permanent deflection versus non-dimensional velocity in Figs. 11 and 14 for plate strips and stiffened panels, respectively. The model couples hydrodynamic forces and structural deformations during abnormal slamming events (ALS) and provides good accuracy by comparison with ALE simulations (refer Part II paper (Yu et al., 2019)). A big advantage of the model is that it bypasses the traditional approach, which focuses on the slamming pressure. It requires only the initial water impact velocity as the main input. The non-dimensional curves in Figs. 11 and 14 are well suited to be utilized in rules and standards for designing against extreme (ALS) slamming loads.

## 8. Conclusions

This Part I of a two-part companion paper proposes a new analytical model for the large inelastic deflection of plates and stiffened panels subjected to extreme water impacts. Flat or nearly flat impacts are considered, where the impact angle between water free surface and the structure should preferably be no larger than  $5^\circ$ . The following conclusions are drawn:

1. The proposed analytical model couples the hydrodynamic pressure and the large plastic structural response during extreme slamming events. To the authors' knowledge, it is the first time that the hydro-plastic slamming problem is solved analytically. The model is verified of good accuracy by comparison with experiments and numerical simulations in the Part II paper.
2. Three deformation stages are assumed for beams and stiffened panels: i.e. the travelling hinge stage 1, the stationary hinge stage 2 and the pure tension stage 3. The travelling hinge concept is introduced in order to not violate theoretically the generalized yield surface given the large and impulsive pressure loading. Stiffened panels are characterized by large web heights and are governed by stages 1 and 2 deformations. Plate strips have large ratios of length over thickness, and are governed by stage 3.
3. In the hydro-plastic regime, the hydrodynamic pressure is found to have two contributions. The first represents an added mass effect, where the added mass is significant and is normally several times the structural mass. The second term comes from the time variation of added mass due to structural modal changes in stage 1. This is different with the pressure in the hydro-elastic regime, where the pressure is associated with only an added-mass effect.
4. The hydro-plastic response of beams and stiffened panels is largely governed by the non-dimensional impact velocity  $V_0 \sqrt{\rho L^3 / (M_0 h / b)}$ . The permanent deflection increases nonlinearly



for stiffened panels that are governed by stages 1 and 2 deformations. The relationship becomes virtually linear for plate strips governed by stage 3.

5. The theory is developed for “unlimited” deformations. In practice, the validity of the model will be limited by fracture due to excessive strain. For unstiffened plates, it is considered that the critical permanent deformation w.r.t. fracture is one order of magnitude larger than the plate thickness while for stiffened plates, it is in the order of the web height.

## Acknowledgments

This work has been funded by the Research Council of Norway (NFR) through the Centers of Excellence funding scheme, project AMOS (Grant number 223254) at the Norwegian University of Science and Technology (NTNU). This support is gratefully acknowledged by the authors.

## References

- Amin, W., Davis, M.R., Thomas, G.A., Holloway, D.S., 2013. Analysis of wave slam induced hull vibrations using continuous wavelet transforms. *Ocean Eng.* 58, 154-166.
- Baarholm, R., 2001. Theoretical and experimental studies of wave impact underneath decks of offshore platforms. Department of Marine Hydrodynamics, Faculty of Marine Technology, Norwegian University of Science and Technology, Trondheim.
- Bereznitski, A., 2001. Slamming: the role of hydroelasticity. *Int Shipbuild Prog* 48, 333-351.
- Bishop, R.E., Price, W.G., 1979. *Hydroelasticity of ships*. Cambridge University Press.
- DNV, 2001. *Offshore Standard DNV-OS-A101, Safety Principals and arrangements*. January.
- DNV, 2014. *Recommended Practice DNV-RP-H103, Modelling and Analysis of Marine Operations*. Det Norske Veritas.
- DNVGL-OTG-13, 2016. *Prediction of air gap for column stabilised units. offshore technical guidance*.
- DNVGL-OTG-14, 2016. *Horizontal wave impact loads for column stabilised units. Offshore Technical Guidance*.
- Faltinsen, O.M., 2000. Hydroelastic slamming. *J. Marine Sci. Technol.* 5, 49-65.
- Faltinsen, O.M., 2005. *Hydrodynamics of high-speed marine vehicles*. Cambridge university press.
- Greco, M., Landrini, M., Faltinsen, O., 2004. Impact flows and loads on ship-deck structures. *Journal of Fluids and Structures* 19, 251-275.
- Hagiwara, K., Yuhara, T., 1974. *Fundamental Study of Wave Impact Load on Ship Bow (1st Report)*. *Journal of the Society of Naval Architects of Japan* 1974, 181-189.
- Henke, D.J., 1994. Transient response of plates to travelling loads with application to slamming damage. *International journal of impact engineering* 15, 769-784.
- Intelligent Engineering, 2010. <http://www.ie-sps.com/news/sps-overlay-to-reduce-slamming-damage>.
- Jiang, J., Olson, M., 1995. Rigid-plastic analysis of underwater blast loaded stiffened plates. *International journal of mechanical sciences* 37, 843-859.
- Jones, N., 1973. Slamming damage, *Journal of Ship Research*, pp. 80-86.
- Jones, N., 2011. *Structural impact*. Cambridge university press.
- Kvalsvold, J., Faltinsen, O.M., 1995. Hydroelastic modelling of wet deck slamming on multihull vessels.
- Lugni, C., Miozzi, M., Brocchini, M., Faltinsen, O.M., 2010. Evolution of the air cavity during a depressurized wave impact. I. The kinematic flow field. *Physics of Fluids* 22, 056101.
- Mei, X., Liu, Y., Yue, D.K.P., 1999. On the water impact of general two-dimensional sections. *Applied Ocean Research* 21, 1-15.

- Schubak, R., Olson, M., Anderson, D., 1993a. Rigid-plastic modelling of blast-loaded stiffened plates—Part I: One-way stiffened plates. *International journal of mechanical sciences* 35, 289-306.
- Schubak, R.B., Olson, M.D., Anderson, D.L., 1993b. Rigid-plastic modelling of blast-loaded stiffened plates—Part I: One-way stiffened plates. *International Journal of Mechanical Sciences* 35, 289-306.
- Schubak, R.B., Olson, M.D., Anderson, D.L., 1993c. Rigid-plastic modelling of blast-loaded stiffened plates—Part II: Partial end fixity, rate effects and two-way stiffened plates. *International Journal of Mechanical Sciences* 35, 307-324.
- Shin, H., Seo, B., Cho, S.-R., 2017. Experimental investigation of slamming impact acted on flat bottom bodies and cumulative damage. *International Journal of Naval Architecture and Ocean Engineering*.
- Symonds, P.S., Mentel, T.J., 1958. Impulsive loading of plastic beams with axial constraints. *Journal of the Mechanics and Physics of Solids* 6, 186-202.
- Symonds, P.S., Yu, T.X., 1985. Counterintuitive Behavior in a Problem of Elastic-Plastic Beam Dynamics. *Journal of Applied Mechanics* 52, 517-522.
- von Karman, T., 1929. The impact on seaplane floats during landing.
- Wagner, H., 1932. Über Stoß- und Gleitvorgänge an der Oberfläche von Flüssigkeiten. *ZAMM-Journal of Applied Mathematics and Mechanics/Zeitschrift für Angewandte Mathematik und Mechanik* 12, 193-215.
- Wierzbicki, T., Suh, M., 1988. Indentation of tubes under combined loading. *International Journal of Mechanical Sciences* 30, 229-248.
- Yamamoto, Y., Iida, K., Fukasawa, T., Murakami, T., Arai, M., Ando, A., 1985. Structural damage analysis of a fast ship due to bow flare slamming. *Int Shipbuild Prog* 32, 124-136.
- Yu, Z., Amdahl, J., 2018. A review of structural responses and design of offshore tubular structures subjected to ship impacts. *Ocean Eng.* 154, 177-203.
- Yu, Z., Amdahl, J., Greco, M., Xu, H., 2019. Hydro-plastic response of beams and stiffened panels subjected to extreme water slamming at small impact angles, Part II: numerical verification and analysis. *Marine Structures*.
- Yu, Z., Amdahl, J., Sha, Y., 2018. Large inelastic deformation resistance of stiffened panels subjected to lateral loading. *Marine Structures* 59, 342-367.
- Zhao, R., Faltinsen, O., 1993. Water entry of two-dimensional bodies. *Journal of Fluid Mechanics* 246, 593-612.

### **Appendix: BEM for the numerical solution of the hydrodynamic problem in Fig. 5.**

The numerical solution of the 2D boundary value problem for the velocity potential  $\varphi$ , sketched in Fig. 5, is briefly described. The problem is governed by the Laplace eq. (7), complemented by the high-frequency free-surface boundary condition eq. (9) along  $x \leq 0$ ,  $x \geq 2L$  and  $z = 0$ , and the impermeability body-boundary condition eq. (10) along  $0 \leq x \leq 2L$  and  $z = 0$ .

The problem for  $\varphi$  is solved with a boundary integral formulation using the Green's second identity, so that the Laplace equation is automatically satisfied. Enforcing the Green's second identity along the domain boundary, integral equations are obtained for the unknowns, i.e.  $\varphi$  along the body and its normal derivative,  $\partial\varphi/\partial n$ , along the free surface. These integral equations are solved numerically using a BEM where the domain boundary (body and free surface) are discretized in straight elements (panels) and in each of them, linear shape functions are used to express  $\varphi$  and  $\partial\varphi/\partial n$ . This allows to estimate analytically the integrals along the panels involved in the discretized version of the integral equations. More details on the BEM method can be found

e.g. in Greco et al. (2004). Fig. A1 presents the BEM solution for  $\varphi$  along the body in the case of uniform and unitary vertical velocity of the body, i.e.  $w_{\text{mode}}$ . This compares well against the analytical solution given by eq. (12).

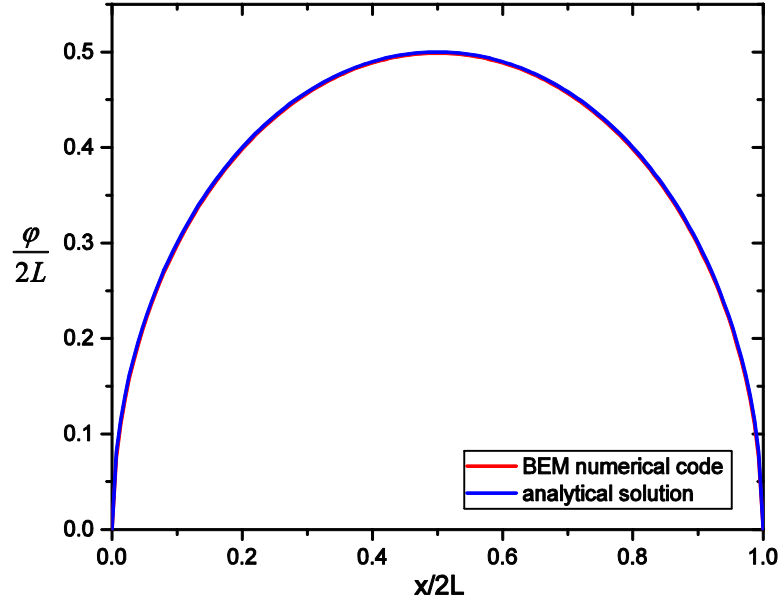


Fig. A1. Velocity potential from BEM and from the analytical solution of BVP in Fig. 5 for uniform and unitary  $w_{\text{mode}}$

The numerical results have been obtained using 150 panels uniformly distributed on the body, the same discretization size is used on the free-surface within a distance equal to  $2L$  from the intersections with the body. Then a panel stretching is introduced to ensure practically zero body perturbation at the far-field edges of the numerical free surface. The same discretization is employed for the BEM results discussed in section 7.1. There, the BEM solution is used to estimate the non-dimensional hydrodynamic parameters  $I_A$  and  $I_B$ .